UCRL-ID-150702

Wölter Instrument – Optical Design

W. W. Nederbragt

U.S. Department of Energy

Lawrence
Livermore
National
Laboratory

October 11, 2002

DISCLAIMER

This work was performed under the auspices of the U. S. Department of Energy by the University of California, Lawrence Livermore National Laboratory under Contract No. W-7405-Eng-48.

Wölter Instrument – Optical Design

Walter Nederbragt

October 11, 2002

TABLE OF CONTENTS:

Contributors:
Jeff Klingmann
Steve Lane
Harry Martz
Mike Pivovaroff

1.0 Introduction

Hundreds of target assemblies (see Figure 1.1) will be constructed annually for use on NIF or OMEGA in the near future. Currently, we do not have the capability to tomographically characterize the target assemblies at the desired resolution. Hence, we cannot verify if an assembly has been assembled correctly. The Engineering Directorate, through the LDRD program, is currently funding an x-ray instruments that could solve this problem. This instrument is based on a Wölter [1] Type-I design. We will refer to this design as the Wölter instrument in the remainder of the report

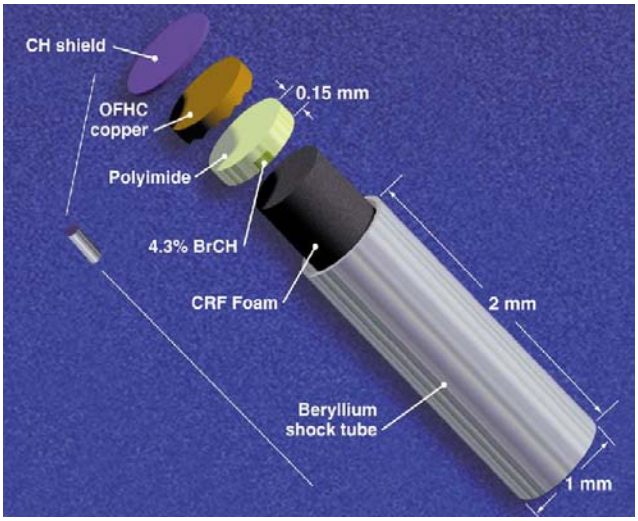

Figure 1.1: One possible configuration of a target assembly

Ideally, the Wölter instrument will create images with sub-micrometer resolution. Moreover, the instrument will have a field-of-view large enough to cover an entire target assembly (up to a 2 mm square), which would eliminate the need to take multiple radiographs to get one complete target image. This report describes the optical design of the Wölter instrument.

2.0 The General Wölter Instrument Design

The Wölter instrument uses two mirrors to focus x-rays that are exiting the target assembly. These x-rays are focussed onto the image plane. The first mirror is hyperbolic and the second mirror is elliptical (see Figure 2.1). By using the configuration shown in Figure 2.1, x-rays that exit the center of the target (this is the right-sided hyperbolic focal point) will be imaged (without blur) at the center of the image plane (this is the right-sided elliptical focal point). X-rays that exit the target off-axis will be imaged at the image plane with a magnification and inverted. Moreover, off-axis points on the target will become blurred at the image plane.

Since target assemblies do not release their own x-rays, an x-ray source is required. We are considering two possible ways of delivering x-rays to the target so that they can pass through the target and be focussed onto the image plane. One method uses condenser optics to collect x-ray photons as they leave the source and project them onto the target (see Figure 2.2). The condenser system consists of two parabolic mirrors. The first parabolic mirror collimates the x-rays emitted from the source. The second parabolic mirror focuses the collimated x-rays back to a small spot at the target. The magnification of the condenser system and the focal spot size of the source determine the size of the spot projected onto the target. The other method does not use a condenser system. Instead the x-ray source is placed directly behind the target (see Figure 2.3). The advantages and disadvantages of these two designs are discussed in Section 8.0.

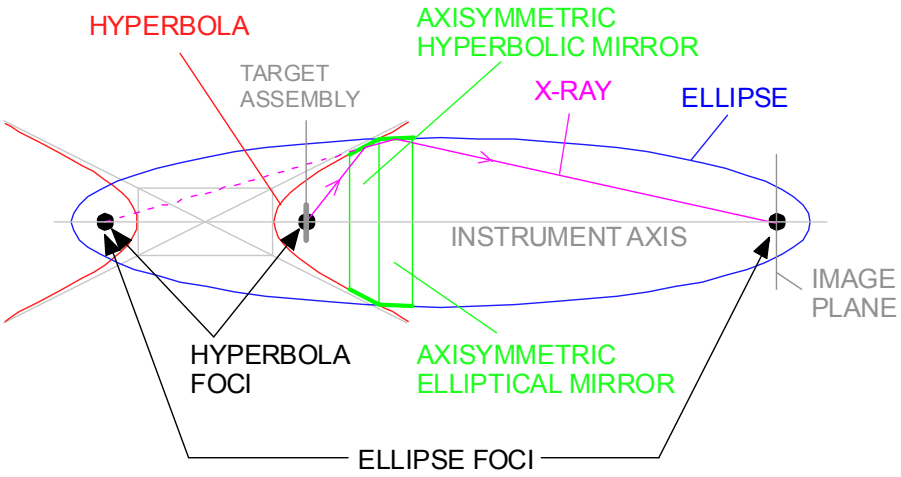

Figure 2.1: Wölter Geometry

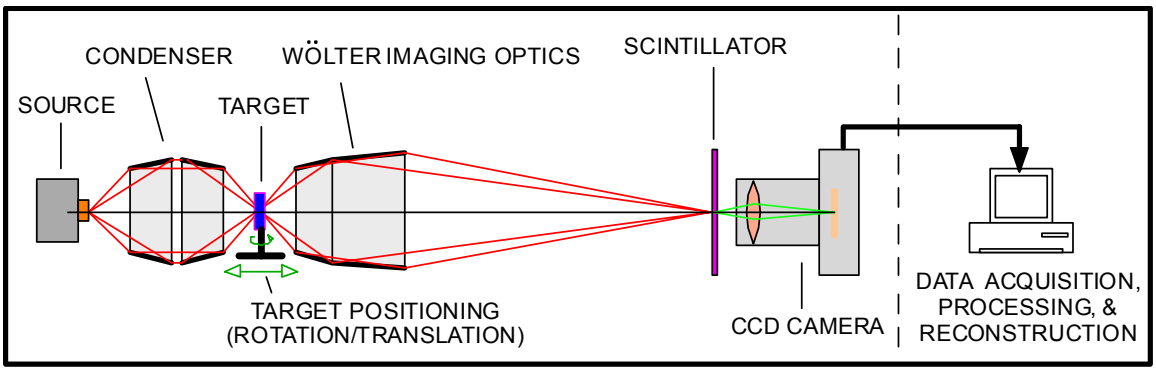

Figure 2.2: Illustration of a Wölter instrument that uses condenser optics

The x-rays that strike the image plane need to be captured for image processing. This is accomplished by placing a scintillator at the image plane. The scintillator converts x-ray photons into visible light. A CCD camera then captures this visible light. CCD cameras have fixed pixel sizes. The camera that we will use has 9-micrometer pixels. Hence, the CCD camera has a fixed resolution of 18-micrometers because of aliasing problems associated with digital sampling. In order to achieve 0.5-micrometer resolution at the target, we need to magnify the image by a minimum of 36 times (0.5 um x 36 = 18 um). The Wölter optics can be designed to do the entire magnification, or the magnification can be accomplished using a combination of Wölter optics and a lens system on the visible light side of the scintillator. It should be noted that the scintillator also has resolution limits. The scintillator resolution is approximately equal to its thickness. For example, a scintillator with 6-micrometer resolution should have a thickness no greater than 6-micrometers. The conversion efficiency of a scintillator is also proportional to its thickness; hence, we do not want to make the scintillator too thin. Table 2.1 lists the magnification possibilities that we considered for the Wölter instrument.

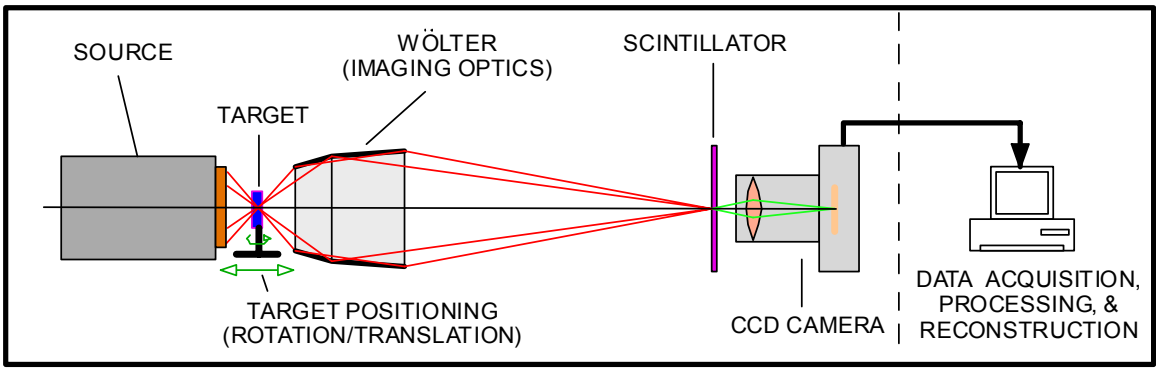

Figure 2.3: Illustration of a Wölter instrument that does not use condenser optics

Resolution at the target	Wölter magnification	Scintillator resolution	Optical magnification	CCD required resolution	CCD required pixel size
0.5 um	36x	18 um	1x	18 um	9 um
	18x	9 um	2x		
	12x	6 um	3x		
	9x	4.5 um	4x		
	6x	3 um	6x		
	3x	1.5 um	12x		

Table 2.1: Magnification options

Our CCD camera has a 2000 pixel by 3000 pixel imaging chip. This results in a coverage of 0.5-millimeter by 0.75-millimeter (2000 x 9 um / 36 = 0.50 mm and 3000 x 9 um / 36 = 0.75 mm) at the target assembly. Since the targets are usually equal to or larger than 1 millimeter in length or diameter, we cannot obtain a radiograph of the entire target at one time with this CCD camera. In order to cover the entire target, we will need to take multiple images of different sections of the part and combine them into one image. This is commonly referred to as tiling (see Figure 2.4).

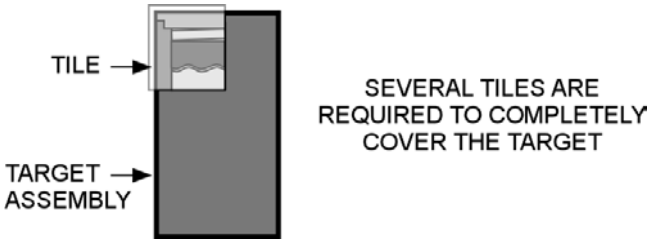

Figure 2.4: Several small radiographs tiled together can be used to create a complete target assembly radiograph

Even if we had a CCD camera that could acquire high-resolution data over the entire target, we still may have to rely on tiling. If the resolution obtained by the Wölter instrument is unacceptable over the full field-of-view but is acceptable over part of the field-of-view, then we can use the acceptable portion and tiling to make a complete image. Based on the results described in the remainder of this report, it is likely that we will need to tile to improve the resolution.

In the next sections of the report, different Wölter instrument design issues are discussed. These issues strongly affect the performance of the instrument. We believe, based on the analysis results, that the most promising design has the following parameters:

Parameter Description	Value
Use of condenser system	NO
Wölter optics - magnification	12x
Visible magnification (between scintillator and CCD)	3x
Instrument length	5 meters
Maximum collection angle	5.6 degrees
Throughput (solid angle fraction, 1= full hemisphere)	$3x10^{-4}$

Figure 2.5 shows the expected blur versus field-of-view for this design. The design has a blur of almost 10-micrometers at a 1-millimeter field-of-view. This is far from our goal, but it still appears to be the most promising design. Figure 2.6 shows how we determine the blur throughout this document; our method is conservative.

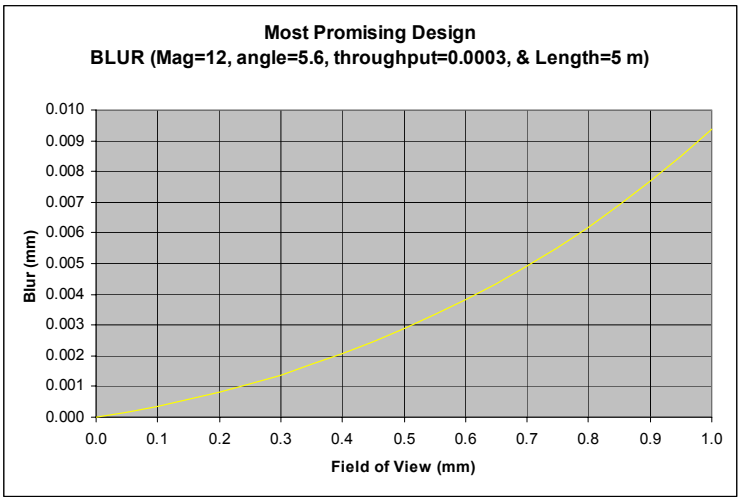

Figure 2.5: Blur versus field of view (diameter) for a promising design

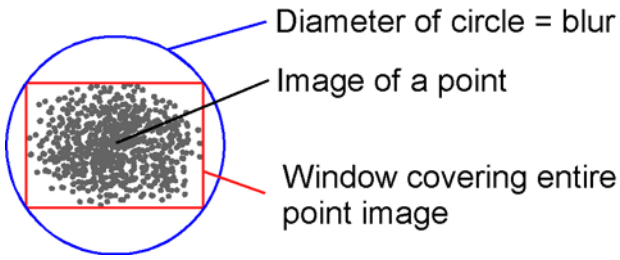

Figure 2.6: Method used to determine blur

3.0 Instrument Magnification

Wölter optical systems can be designed to provide a wide range of magnifications. The magnification is controlled by placement of the optics. The ratio of the optics-to-scintillator distance to the target-to-optics distance provides an approximation of the magnification. Ideally, we would like a magnification of 36. With this magnification, a thicker scintillator (higher efficiency) can be used without compromising the resolution of the instrument. Moreover, no additional magnification is needed between the scintillator and CCD camera. Figure 3.1 illustrates two different instrument designs. Figure 3.1(a) has a higher magnification than Figure 3.1(b). The optics in Figure 3.1(b) must be larger than the optics in Figure 3.1(a) if the same throughput is to be maintained.

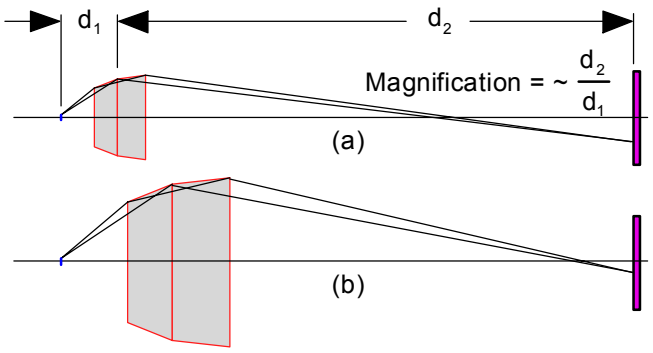

Figure 3.1: Illustration of instruments with two different magnifications (same throughput).

There is a problem with using high magnification. The optical components move closer to the target as the magnification is increased, but the target remains the same size. This causes off-axis points on the target to become more blurred. The higher magnification reduces this effect at the image plane. When both of these effects are linear, they will counteract each other, resulting in the same blur performance. This is the case for a Wölter instrument with low throughput (see Figure 3.3). When the throughput is higher, the off-axis blur becomes higher order (see Figure 3.2). In this case, lowering the magnification improves the blur performance of the instrument. Since a low throughput instrument is not desirable (see Section 6), we want to base our design on the high throughput case. Hence, in our design, we want to reduce the magnification to as low as possible without compromising other aspects of the design.

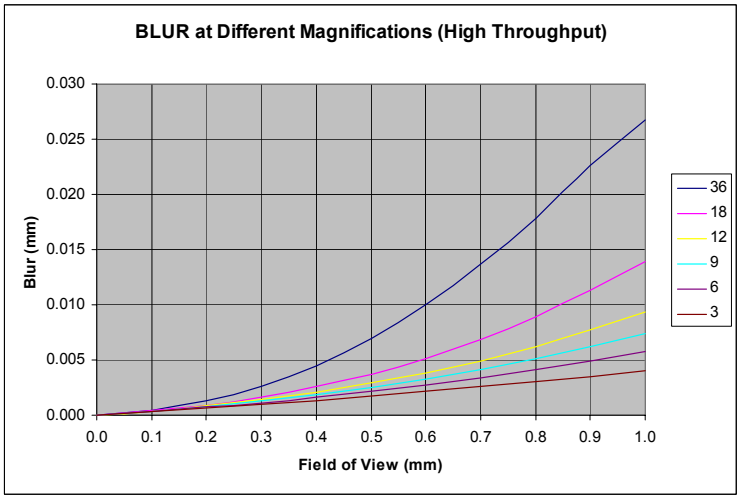

Figure 3.2: Instrument blur for different magnifications at a high throughput ($3x10^{-4}$ solid angle)

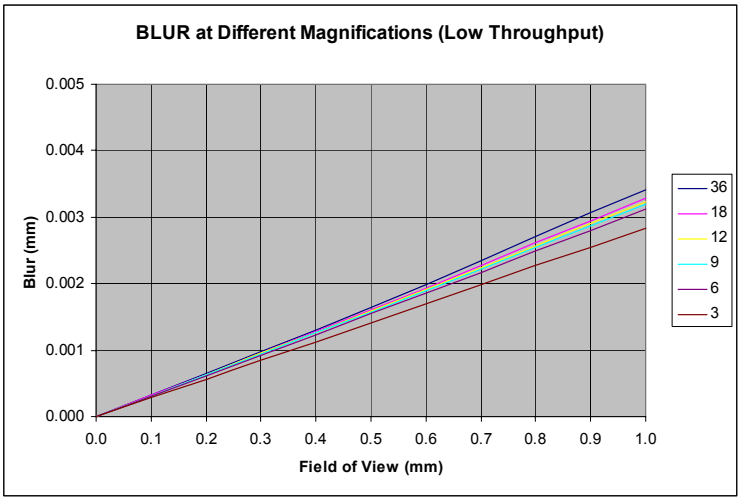

Figure 3.3: Instrument blur for different magnifications at a low throughput ($3x10^{-6}$ solid angle)

4.0 Instrument Length (Scale)

We have a large amount of control when choosing the length of our Wölter instrument. When we increase the length, we want to keep the throughput, magnification, and maximum collection angle the same. This allows us to correctly ascertain the effects of increasing the length. This is done by increasing or decreasing all the dimensions of the instrument at the same rate (i.e., scaling the design – see Figure 4.1). From a ray-tracing standpoint, there are no bounds on the scale. From a mechanical standpoint, it becomes increasingly difficult to fabricate the instrument as the length increases because vibration isolation and thermal isolation become problematic. From a radiography standpoint, the increased photon attenuation caused by gases along the longer instrument reduces the efficiency of the instrument. Hence, there is a point in which increasing the scale becomes impractical.

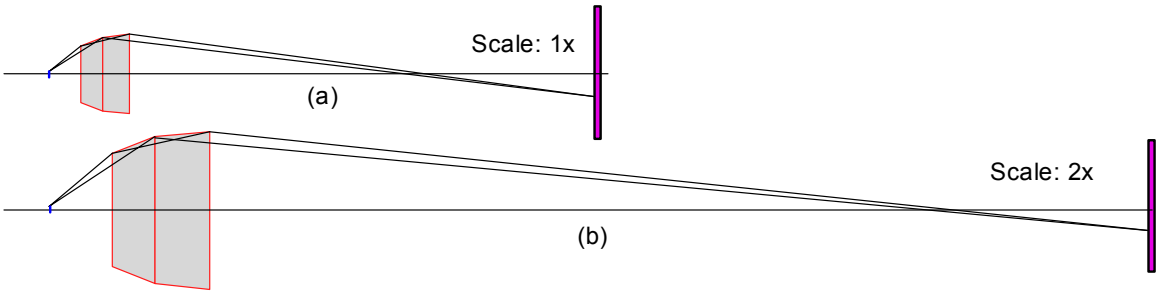

Figure 4.1: Illustration of similar instruments with different scales.

From a ray-tracing standpoint, an increase in the instrument scale also causes an increase in blur. For example, given a blur of 0.002 millimeters for an off axis position of 0.2 millimeters, doubling the instrument size would result in a blur of 0.004 millimeters for an off axis position of 0.4 millimeters. However, the target, which is not part of the instrument, remains the same size, so the field of view does not need to change size. Hence, it may be possible to reduce the blur for a given target assembly by increasing the size of the instrument. If the blur increases linearly with off-axis position, then the blur will remain the same (i.e., no improvement) as we scale the instrument. This is the case for a Wölter instrument with low throughput (see Figure 4.3). When the throughput is higher, the off-axis blur becomes higher order (see Figure 4.2). In this case, increasing the scale improves the blur performance of the instrument. Since a low throughput instrument is not desirable (see Section 6), we want to base our design on the high throughput case. Hence, in our design, we want to increase the scale as much as possible without compromising other aspects of the design.

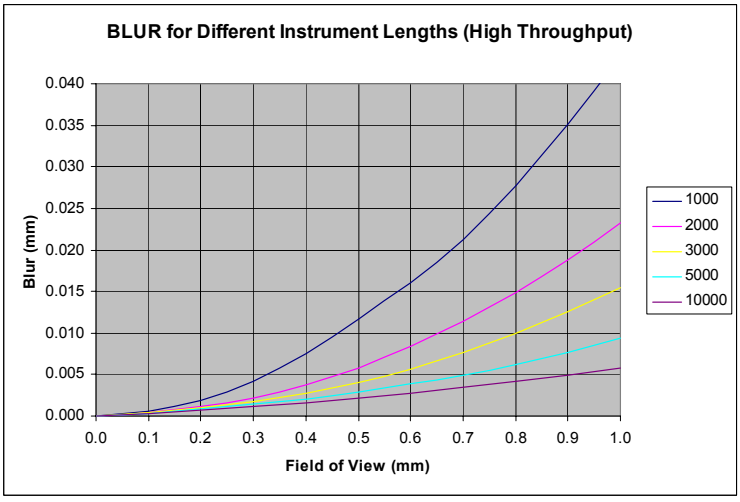

Figure 4.2: Blur for different instrument lengths at a high throughput ($3x10^{-4}$ solid angle)

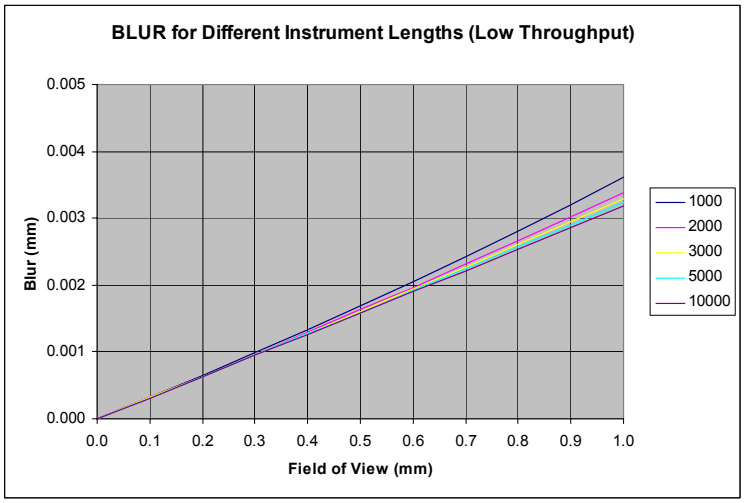

Figure 4.3: Blur for different instrument lengths at a low throughput ($3x10^{-6}$ solid angle)

5.0 Maximum Collection Angle

Changing the maximum collection angle (see Figure 5.1) can strongly impact the performance of our instrument. When comparing different collection angles, the throughput (see Section 6.0) should be held constant to make the comparison legitimate. It should be noted that increasing the collection angle increases the reflection angles at the mirror surfaces. Hence, there is a maximum practical collection angle. This angle is approximately 3.3 times larger than the maximum permissible reflection angle for the geometries that we are studying. For example, if the largest permissible reflection angle is 1.7 degrees, then the maximum collection angle is approximately 5.6 degrees. If a condenser optical system is used, then the maximum collection angle is controlled by the reflection angles on the condenser optics (see Section 8).

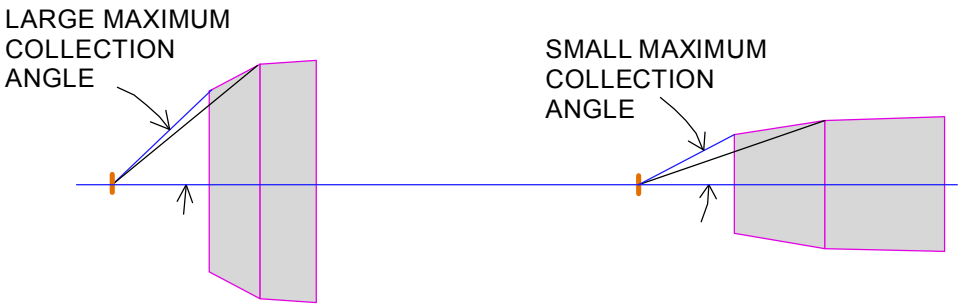

Figure 5.1: Illustration of two different collection angles

Changing the maximum collection angle on a high-throughput design (solid angle = $3x10^{-4}$) strongly affects the blur characteristics; the blur performance is greatly improved when the collection angle is increased (see Figure 5.2). Changing the maximum collection angle on a low-throughput design (solid angle = $3x10^{-6}$) also strongly affects the blur characteristics. However, in this case, the blur performance is significantly reduced when the collection angle is increased (see Figure 5.3). Since we need high throughput; we want to maximize the collection angle.

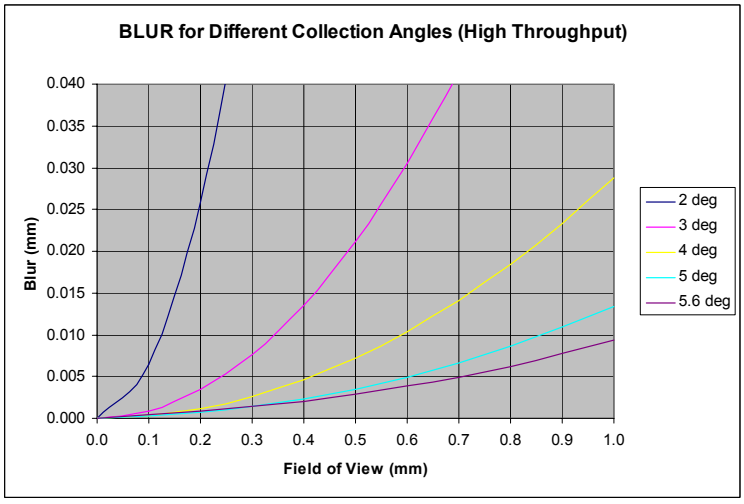

Figure 5.2: Blur for different instrument collection angles at a high throughput ($3x10^{-4}$ solid angle)

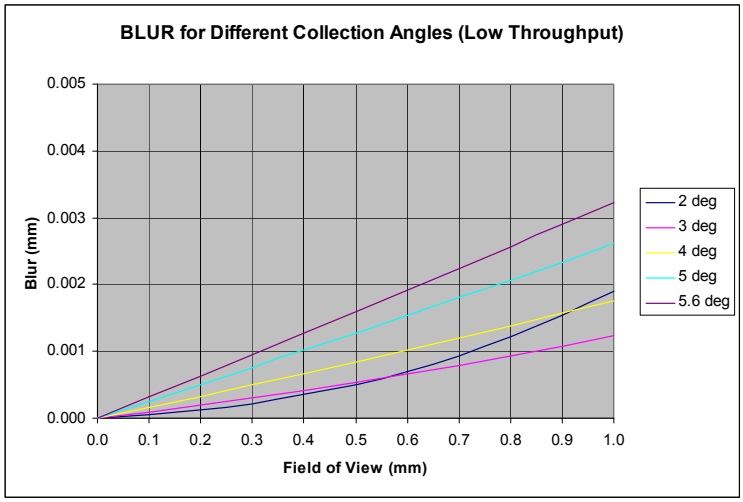

Figure 5.3: Blur for different instrument collection angles at a low throughput ($3x10^{-6}$ solid angle)

6.0 Instrument Throughput

The throughput of an instrument determines how long it will take to acquire an image. Ideally, we want to acquire an image instantly; hence, we want infinite throughput. Unfortunately, portable x-ray sources (tube sources) have limited photon fluxes. Our Machlett source has a photon flux of approximately 4×10^{14} photons per second per square millimeter (in 5% bandwidth at 8 keV using a copper anode). The photon collection capability of the optics also greatly affects the throughput. This photon collection capability is easy to express using solid angles (see Figure 6.1 and Equation 6.1). A solid angle is the fraction of source photons that are collected by the optics. Obviously, for maximum throughput, we want this number to be as large as possible (a value of one represents collection over an entire hemisphere). This can be done by increasing the maximum collection angle (θ_1) and increasing $\theta_1 - \theta_2$. To help illustrate the need for high throughput, Table 6.1 gives the expected image time for a Wölter instrument using a Machlett source without a condenser that has a solid angle of 3×10^{-4}. Note: the CCD camera needs 1.6×10^{11} photons to create an adequate image (10,000 photons per pixel) that covers a square millimeter of the target at a resolution of 0.5 micrometers.

$$\text{Solid Angle} = \cos(\theta_2) - \cos(\theta_1) \qquad \text{(eq 6.1)}$$

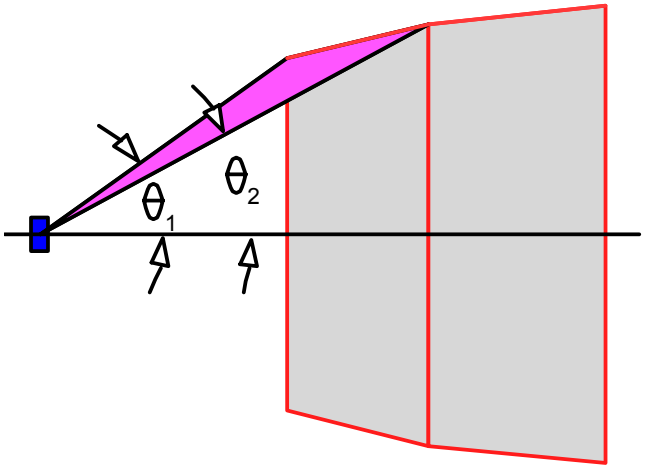

Figure 6.1: θ_1 and θ_2 Control instrument throughput

Instrument section	Efficiency	Photons/sec
Source		4.00E+14
Target transmittion	0.1	4.00E+13
Optical photon collection (solid angle)	0.0003	1.20E+10
Hyperbolic optic reflection efficiency	0.4	4.80E+09
Elliptical optic reflection efficiency	0.4	1.92E+09
Scintillator conversion efficiency	0.05	9.60E+07

Number of photons needed at CCD camera =	1.60E+11
Time in seconds needed to acquire an image =	1666.67
Time in minutes needed to acquire an image =	27.78
Time in hours needed to acquire an image =	0.4630

Table 6.1: Time needed to acquire an image

It takes approximately 30 minutes to acquire an image with a solid angle of $3x10^{-4}$. With a solid angle of $3x10^{-6}$ it will take 3000 minutes to acquire the same image. Figure 6.2 shows the blur at multiple throughput values for a Wölter instrument with a 5.6-degree maximum collection angle. The "1x" line in the figure represents a solid angle of $3x10^{-6}$. The other lines are multiples of that value. As can be seen in the figure, the blur doesn't increase much with increased throughput until we get to 128x ($3.84x10^{-4}$ solid angle). Hence, increasing the throughput to 100x seems logical because the adverse effects are small.

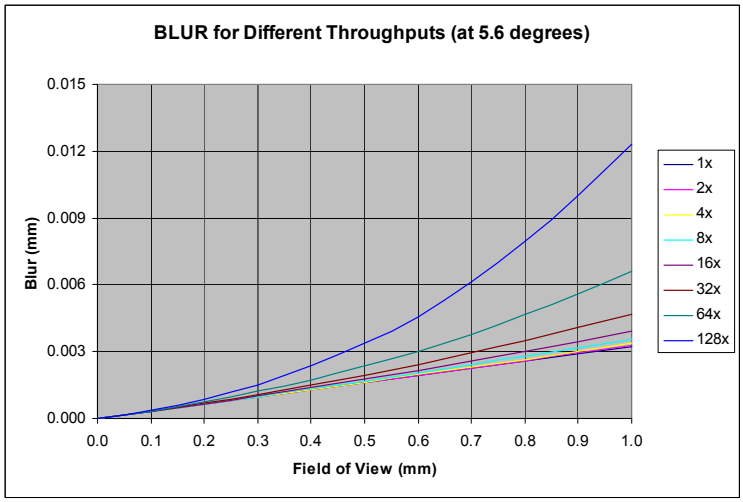

Figure 6.2: Blur at different instrument throughputs (collection angle is fixed at 5.6 degrees)

Figure 6.3 shows the blur at multiple throughput values for a Wölter instrument with a 3-degree maximum collection angle. The "1x" line in that figure is also associated with a throughput of $3x10^{-6}$. The other lines are multiples of that value. As can be seen in the figure. The blur begins to significantly increase at 16x ($4.8x10^{-5}$ solid angle). Hence, the throughput of this instrument deteriorates rapidly as the throughput is increased.

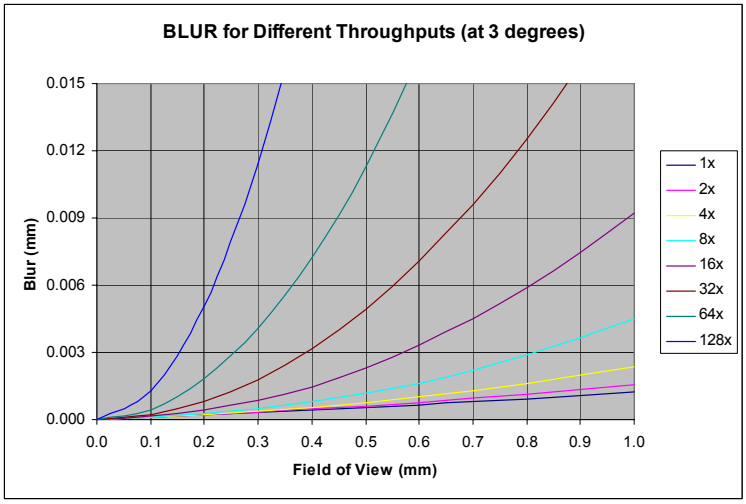

Figure 6.3: Blur at different instrument throughputs (collection angle is fixed at 3.0 degrees)

7.0 Multilayer Coatings

Multilayer coatings make it possible to increase the reflection angle of our Wölter optics at a specific x-ray energy (8 keV in our case). Figure 7.1 illustrates the purpose of the multilayers. As was shown in Section 5, increasing the maximum collection angle improves the performance of a Wölter instrument when the throughput is "high." Increasing the collection angle increases the reflection angle of the Wölter optics; hence, if multilayers can increase the reflection angle, then we can increase the collection angle and get a better instrument design.

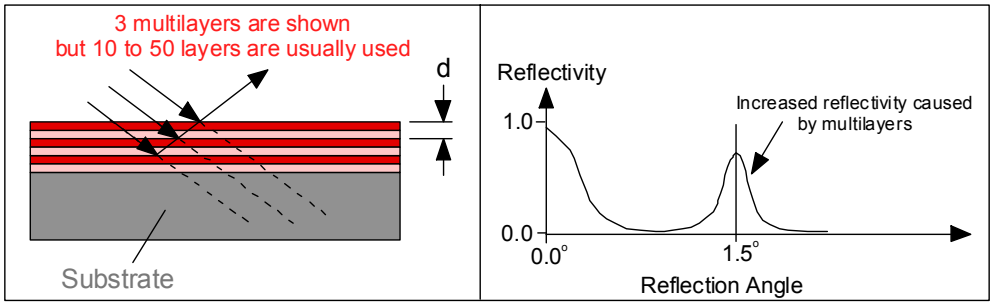

Figure 7.1: Multilayer illustration

Figure 7.2 illustrates the effect that the number of layers has on the reflection properties. As we increase the number of layers, the reflectivity improves, but the Full Width Half Maximum (FWHM) decreases.

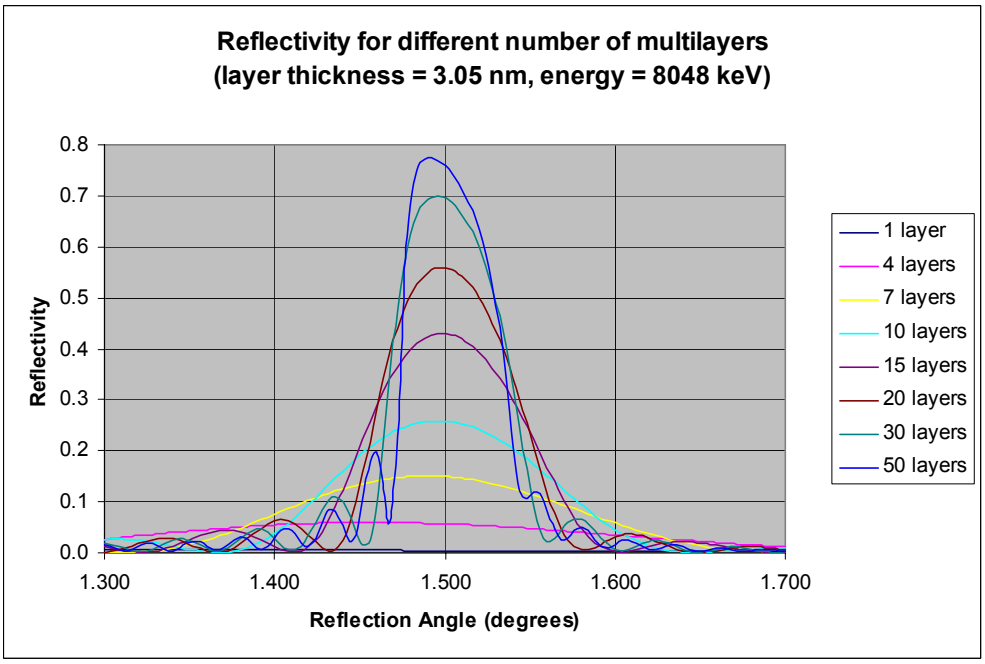

Figure 7.2: Comparison of reflectivity for a different numbers of layers [2].

Multilayers greatly improve the reflectivity at a particular reflection angle for a given x-ray energy (8 keV in our case), but the reflectivity decreases quickly as we deviate from that reflection angle. Since we are trying to image parts that extend beyond the main optical axis, each surface point on the Wölter optics will see a large spectrum of reflection angles. Many of theses x-rays will not be reflected (see Figure 7.3). Figure 7.4 shows the blur associated with imaging off-axis points. The multilayers only reflect a portion of the available photons; this results in the "cone" effect shown. The reduction in efficiency caused by the multilayers versus off-axis location is shown in Figure 7.5 for the "most promising design."

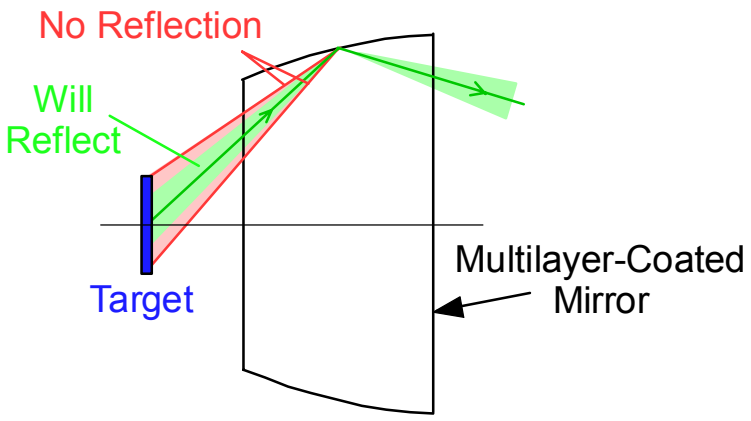

Figure 7.3: Not all X-rays will be reflected

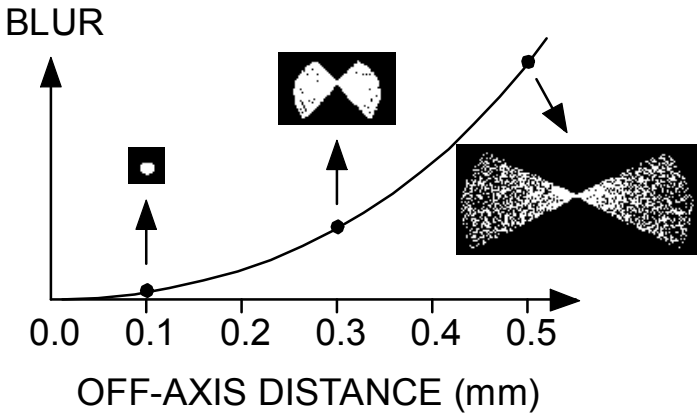

Figure 7.4: Illustrates the reduced throughput for off-axis points caused by the multilayers

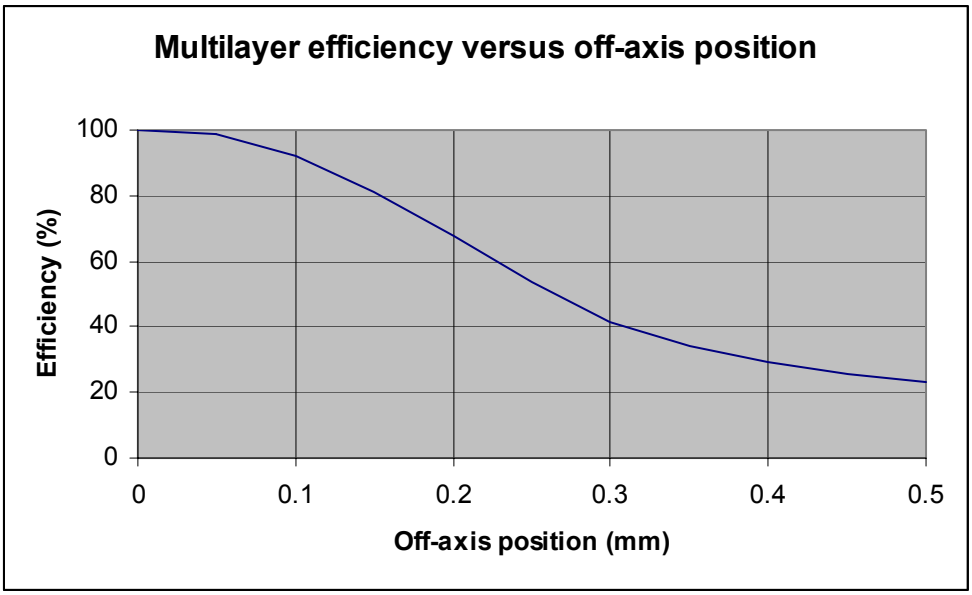

Figure 7.5: Reduction in efficiency caused by the multilayers versus off-axis location for "most promising design" – in this graph, the multilayers are assumed to have a 100% probability of photon reflection at the on-axis angle of incidence (the nominal reflection angle).

8.0 Use of Condenser Optics

The condenser optical system collects the x-rays that are emitted from our source and directs them back onto the target. This is done using two parabolic mirrors. The first mirror collimates the source x-rays. The second mirror directs the collimated x-rays toward the target. The condenser system can be designed to magnify or reduce the size of the source. The true size of the source can be projected onto the target by using a condenser system with a magnification of one. This is the simplest condenser design because both parabolic mirrors are identical. The expected reflection angles for this design are shown in Figure 8.1. As can be seen in the figure, the condenser optics have the highest reflection angle (1.5 degrees). The Wölter optics are limited to reflection angles of approximately 0.8 degrees. Ideally, we want to maximize the reflection angles on the Wölter optics because we want to maximize the maximum collection angle (see Section 5.0). Therefore, the condenser system limits the performance of the Wölter system.

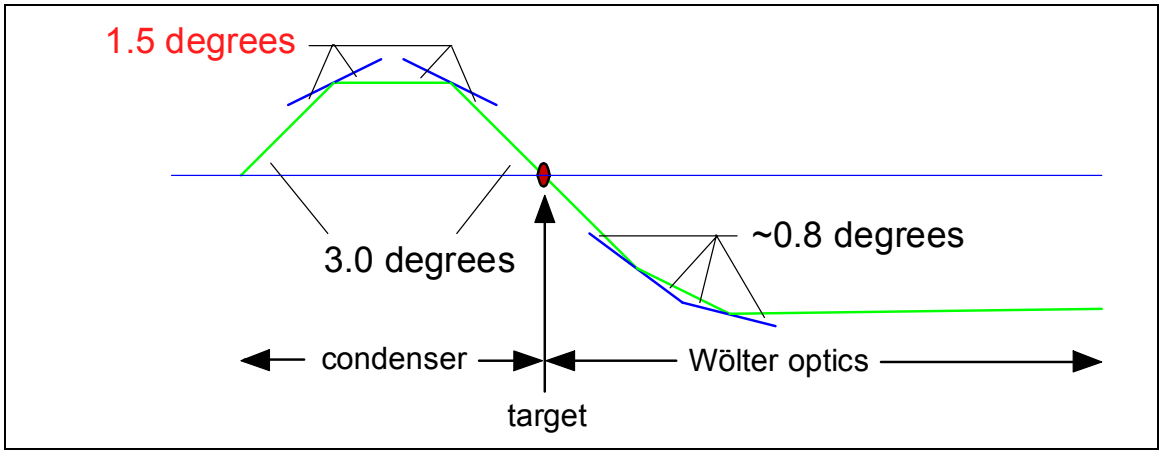

Figure 8.1: Reflection angles for a Wölter design with a 1x-magnification condenser system.

If a small source is used, a high condenser magnification can be used to magnify the source spot that is projected onto the target. Assuming the source photon flux is constant, a smaller source will result in a reduction of throughput. Moreover, the reflection angles at the Wölter optics become even smaller because of the increase in magnification at the condenser. Figure 8.2 illustrates this point. Therefore, this condenser design will perform poorly.

If a large source is used, an image-reducing condenser can be used to reduce the source spot that is projected onto the target. Assuming the source photon flux is constant, a larger source will result in an increase of throughput. Unfortunately the reflection angle at the second parabolic mirror still limits the reflection angles at the Wölter optics. Figure 8.3 illustrates this point.

The three condenser designs limit the maximum collection angle of the Wölter optics. Moreover, every reflection off of a mirror reduces the efficiency of our system. Since we want to maximize the collection angle and the throughput, a design that does not use a condenser system seems appropriate. Figure 8.4 shows the reflection angles associated with this design. Without a condenser, we will need a bigger source to cover the entire target. The source size needed for a condenser-free design is discussed in Section 9.

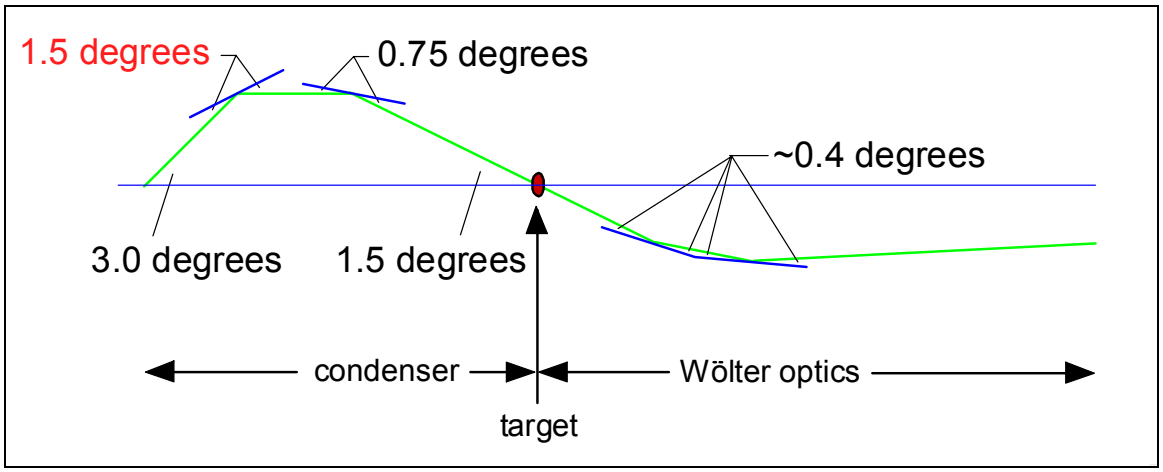

Figure 8.2: Reflection angles for a Wölter design with a 2x-magnification condenser system.

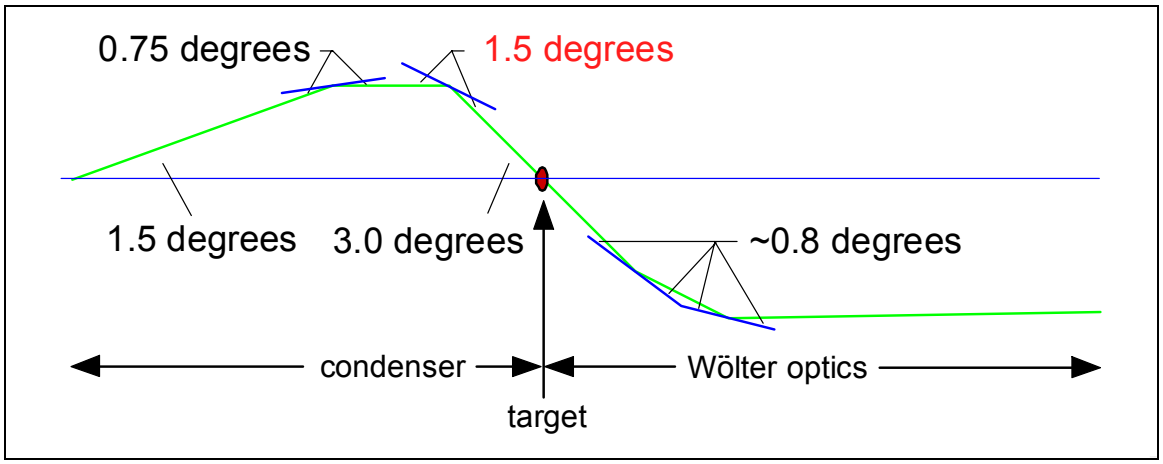

Figure 8.3: Reflection angles for a Wölter design with a 2x-reduction (0.5x magnification) condenser system.

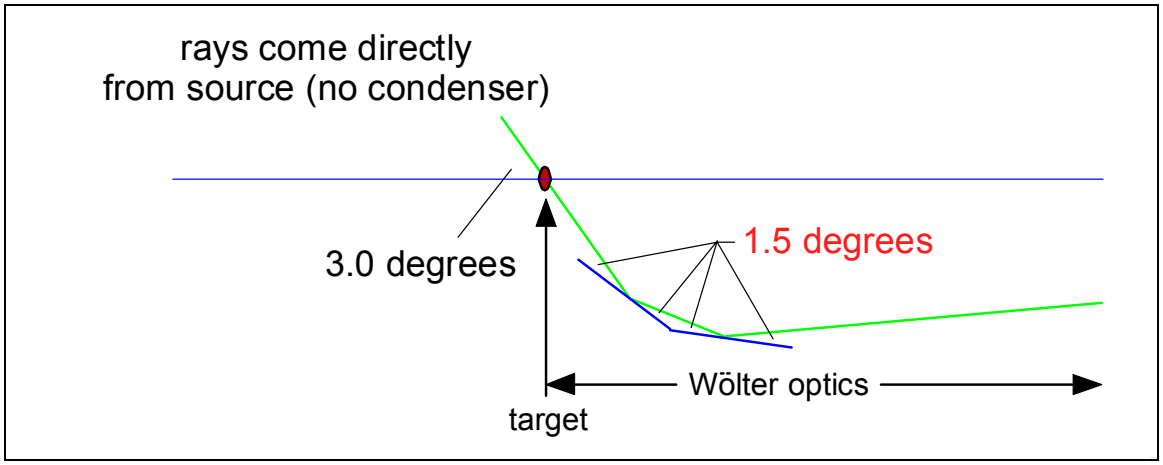

Figure 8.4: Reflection angles for a Wölter design without a condenser system.

9.0 Source Issues

If a condenser system is used, then the magnification or reduction caused by the condenser optics controls the source spot projected onto the target. If a condenser-free design is used, then the source is placed directly behind the target. The distance from the source focal spot to the target determines the size of the source. If the source could be placed infinitesimally close to the target, then the source would need to be the same size as the target to completely cover the target. The required source increases as the source is placed father from the target. Figures 9.1 and 9.2 illustrate this point. Figure 9.2 gives the required source size for various source-to-target distances.

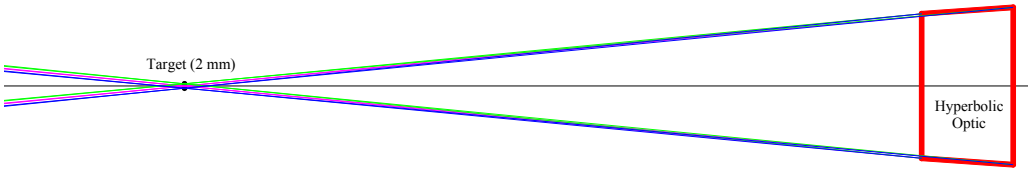

Figure 9.1: Shows the rays that will be collected by the first Wölter optic.

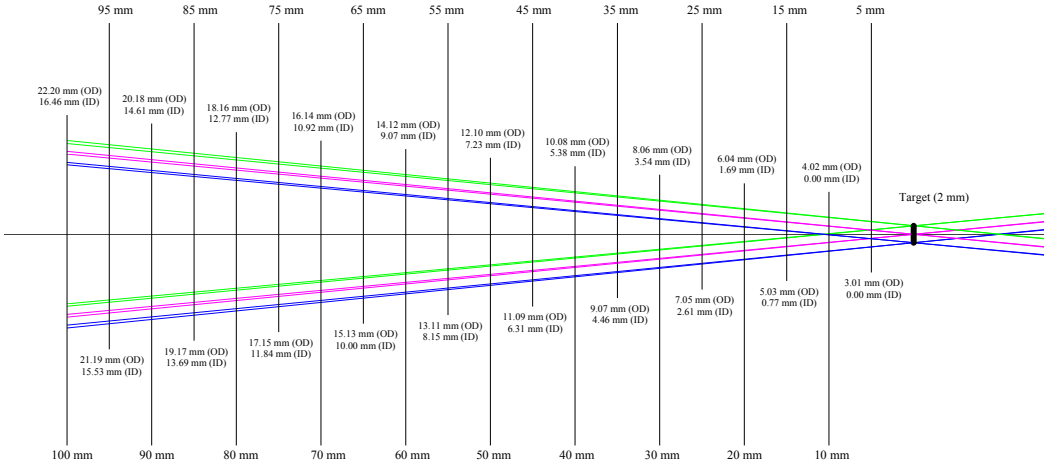

Figure 9.2: shows an enlargement of the left side of Figure 9.1. The required source size is given for different source-to-target distances.

The difference in using a large source placed farther from the target or a small source placed close to the target is insignificant if the x-ray fluxes for both sources are the same. The same number of x-ray photons make it through the instrument. This point is illustrated in Figure 9.3. In Figure 9.3(a), the source is infinitesimally close to the target. The photons that make it though the instrument originate from the center of the source. In Figure 9.3(b), the source is placed about 25 millimeters behind the target. The number of photons that make it through the instrument is the same, but the photons are distributed over a large ring.

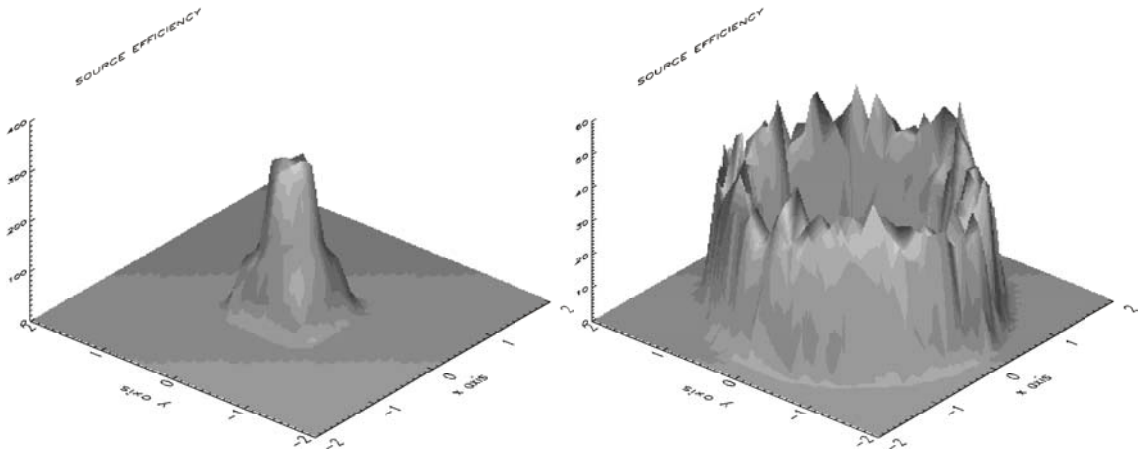

(a) (b)

Figure 9.3: Source efficiency plots

Due to the size and shape of available x-ray sources, it will be difficult if not impossible to place an appropriate source within five millimeters of the target. It is more likely that the source will be at least 25 millimeters away from the target. Therefore, the source will need to be large. If the source provides the same flux as smaller sources, then it will require a lot of power to operate. Moreover, it will generate a lot of heat near the target, which could cause material expansion problems. Finding a large source with high flux may also be a problem. Regardless of these issues, the condenser-less design makes more sense for this prototype; hence, we are staying with this design.

10.0 Conclusion

Based on the information presented, we believe the most practical design does not use a condenser optical system, has a Wölter magnification of 12x, has a maximum collection angle of 5.6 degrees, has a solid angle (throughput) of 3×10^{-4}, and is 5.0 meters long.

11.0 Bibliography

1. Wölter, H., "Mirror Systems with Grazing Incidence as Image-Forming Optics for X-rays," Ann Physik, Vol. 10, 94, 1952.

2. http://www-cxro.lbl.gov/optical_constants/multi2.html

APPENDIX A: BLUR DATA

The following tables contain the data used in many of the figures in the report. These data were obtained using an Excel spreadsheet programmed to trace rays (see Appendix F). Figure 2.5 uses one of the columns in Table A.1 to show the blur of the most promising design (Wmag=12). Figures 3.2 and 3.3 use data from Table A.1 to compare blur characteristics at different Wölter magnifications. Figures 4.2 and 4.3 use data from Table A.2 to compare blur characteristics at different instrument lengths (scales). Figures 5.2 and 5.3 use data from Table A.3 to compare blur characteristics for instrument designs with different collection angles. Figure 6.2 uses data from Table A.4 to demonstrate the effect of increasing the blur when the instrument has a 5.6-degree collection angle. Figure 6.3 uses data from Table A.5 to demonstrate the effect of increasing the blur when the instrument has a 3.0-degree collection angle.

Length total	5000	5000	5000	5000	5000	5000	5000	5000	5000	5000	5000	5000
bc	4.69	9.79	14.58	19.03	29.53	64.00	4.58	9.47	14.49	19.48	31.08	67.75
Wmag	36	18	12	9	6	3	36	18	12	9	6	3
Theta_cf	5.6	5.6	5.6	5.6	5.6	5.6	5.6	5.6	5.6	5.6	5.6	5.6
delta_c	0.179	0.179	0.179	0.179	0.179	0.179	0.00176	0.00176	0.00176	0.00176	0.00176	0.00176
solid angle	0.000300	0.000300	0.000300	0.000300	0.000300	0.000300	0.000003	0.000003	0.000003	0.000003	0.000003	0.000003
refl angle	1.52	1.58	1.60	1.60	1.68	1.87	1.38	1.44	1.48	1.51	1.62	1.83
length CD	33.2	63.0	89.5	113.3	154.2	236.1	0.3	0.6	0.9	1.1	1.5	2.4
dia CD	25.5	49.7	72.7	94.5	135.1	236.5	26.4	51.4	75.1	97.6	139.5	244.3
error 0 mm	0	0	0	0	0	0	0	0	0	0	0	0
error 0.1 mm	0.0005	0.0004	0.0004	0.0003	0.0003	0.0003	0.0003	0.0003	0.0003	0.0003	0.0003	0.0003
error 0.2 mm	0.0013	0.0009	0.0008	0.0008	0.0007	0.0006	0.0006	0.0006	0.0006	0.0006	0.0006	0.0006
error 0.3 mm	0.0026	0.0016	0.0014	0.0013	0.0011	0.0009	0.0010	0.0010	0.0009	0.0009	0.0009	0.0008
error 0.4 mm	0.0045	0.0026	0.0021	0.0018	0.0016	0.0013	0.0013	0.0013	0.0013	0.0013	0.0012	0.0011
error 0.5 mm	0.0070	0.0037	0.0029	0.0025	0.0021	0.0017	0.0016	0.0016	0.0016	0.0016	0.0015	0.0014
error 0.6 mm	0.0100	0.0051	0.0038	0.0033	0.0027	0.0021	0.0020	0.0019	0.0019	0.0019	0.0019	0.0017
error 0.7 mm	0.0137	0.0069	0.0049	0.0041	0.0034	0.0026	0.0023	0.0023	0.0022	0.0022	0.0022	0.0020
error 0.8 mm	0.0178	0.0090	0.0062	0.0051	0.0041	0.0030	0.0027	0.0026	0.0026	0.0025	0.0025	0.0023
error 0.9 mm	0.0226	0.0113	0.0077	0.0062	0.0049	0.0035	0.0031	0.0029	0.0029	0.0029	0.0028	0.0026
error 1.0 mm	0.0267	0.0139	0.0094	0.0074	0.0057	0.0040	0.0034	0.0033	0.0032	0.0032	0.0031	0.0028

Table A.1: Data for comparing blur at different Wölter magnifications

Length total	1000	2000	3000	5000	10000	1000	2000	3000	5000	10000
bc	2.885559327	5.785046	8.691396	13.3	29.15009	2.886002	5.790283	8.691	13.3	29.15
Wmag	12	12	12	12	12	12	12	12	12	12
Theta_cf	5.6	5.6	5.6	5.6	5.6	5.6	5.6	5.6	5.6	5.6
delta_c	0.179	0.179	0.179	0.179	0.179	0.00176	0.00176	0.00176	0.00176	0.00176
solid angle	0.000300	0.000300	0.000300	0.000300	0.000300	0.000003	0.000003	0.000003	0.000003	0.000003
refl angle	1.59	1.59	1.59	1.52	1.60	1.48	1.48	1.48	1.40	1.49
length CD	17.9	35.8	53.7	89.3	179.1	0.2	0.4	0.5	0.9	1.8
dia CD	14.5	29.1	43.6	72.7	145.4	15.0	30.0	45.0	75.1	150.1
error 0 mm	0	0	0	0	0	0	0	0	0	0
error 0.1 mm	0.0006	0.0004	0.0004	0.0004	0.0003	0.0003	0.0003	0.0003	0.0003	0.0003
error 0.2 mm	0.0019	0.0012	0.0010	0.0008	0.0007	0.0006	0.0006	0.0006	0.0006	0.0006
error 0.3 mm	0.0042	0.0022	0.0017	0.0014	0.0012	0.0010	0.0010	0.0010	0.0009	0.0009
error 0.4 mm	0.0074	0.0038	0.0027	0.0021	0.0016	0.0013	0.0013	0.0013	0.0013	0.0013
error 0.5 mm	0.0116	0.0058	0.0040	0.0029	0.0022	0.0017	0.0016	0.0016	0.0016	0.0016
error 0.6 mm	0.0160	0.0084	0.0056	0.0038	0.0028	0.0020	0.0020	0.0019	0.0019	0.0019
error 0.7 mm	0.0212	0.0114	0.0076	0.0049	0.0034	0.0024	0.0023	0.0023	0.0022	0.0022
error 0.8 mm	0.0277	0.0149	0.0099	0.0062	0.0041	0.0028	0.0027	0.0026	0.0026	0.0025
error 0.9 mm	0.0350	0.0188	0.0125	0.0077	0.0049	0.0032	0.0030	0.0030	0.0029	0.0029
error 1.0 mm	0.0433	0.0233	0.0155	0.0094	0.0058	0.0036	0.0034	0.0033	0.0032	0.0032

Table A.2: Data for comparing blur at different instrument lengths (scale)

Length total	5000	5000	5000	5000	5000	5000	5000	5000	5000	5000
bc	3.988610282	7.020071	9.978172	12.79449	13.3	3.99	7.02	9.98	12.79	14.31399
Wmag	12	12	12	12	12	12	12	12	12	12
Theta_cf	2	3	4	5	5.6	2	3	4	5	5.6
delta_c	0.575	0.3487	0.2545	0.2012	0.179	0.00493	0.003286	0.002465	0.001972	0.00176
solid angle	0.000300	0.000300	0.000300	0.000300	0.000300	0.000003	0.000003	0.000003	0.000003	0.000003
refl angle	0.77	0.96	1.19	1.44	1.52	0.45	0.75	1.04	1.31	1.47
length CD	857.7	321.1	176.7	112.4	89.3	7.2	3.1	1.8	1.1	0.9
dia CD	19.1	35.6	50.3	64.4	72.7	26.8	40.2	53.6	67.0	75.1
error 0 mm	0	0	0	0	0	0	0	0	0	0
error 0.1 mm	0.0065	0.0008	0.0003	0.0003	0.0004	0.0001	0.0001	0.0002	0.0003	0.0003
error 0.2 mm	0.0259	0.0034	0.0011	0.0008	0.0008	0.0001	0.0002	0.0003	0.0005	0.0006
error 0.3 mm	0.0581	0.0076	0.0026	0.0014	0.0014	0.0002	0.0003	0.0005	0.0008	0.0009
error 0.4 mm	0.1029	0.0135	0.0046	0.0023	0.0021	0.0003	0.0004	0.0007	0.0010	0.0013
error 0.5 mm	0.1602	0.0212	0.0072	0.0034	0.0029	0.0005	0.0005	0.0008	0.0013	0.0016
error 0.6 mm	0.2297	0.0305	0.0103	0.0049	0.0038	0.0007	0.0007	0.0010	0.0015	0.0019
error 0.7 mm	0.3112	0.0414	0.0141	0.0066	0.0049	0.0009	0.0008	0.0012	0.0018	0.0022
error 0.8 mm	0.4044	0.0541	0.0184	0.0086	0.0062	0.0012	0.0009	0.0014	0.0021	0.0026
error 0.9 mm	0.5001	0.0684	0.0233	0.0109	0.0077	0.0015	0.0011	0.0016	0.0023	0.0029
error 1.0 mm	0.5861	0.0845	0.0287	0.0134	0.0094	0.0019	0.0012	0.0018	0.0026	0.0032

Table A.3: Data for comparing blur for instruments with different maximum collection angles

Length total	5000	5000	5000	5000	5000	5000	5000	5000
bc	13.3	13.3	13.3	13.3	13.3	13.3	13.3	13.3
Wmag	12	12	12	12	12	12	12	12
Theta_cf	5.6	5.6	5.6	5.6	5.6	5.6	5.6	5.6
delta_c	0.00176	0.003525	0.00705	0.01411	0.028254	0.056652	0.11389	0.23018
solid angle	0.000003	0.000006	0.000012	0.000024	0.000048	0.000096	0.000192	0.000384
refl angle	1.402107207	1.403283	1.40563	1.410323	1.419701	1.438424	1.475742	1.549826
length CD	0.896700641	1.79556	3.589279	7.176083	14.3397	28.63952	57.17287	114.3255
dia CD	75.07008515	75.04647	74.99932	74.90487	74.71565	74.33574	73.56995	72.01395
error 0 mm	0.0000	0.0000	0.0000	0.0000	0.0000	0.0000	0.0000	0.0000
error 0.1 mm	0.0003	0.0003	0.0003	0.0003	0.0003	0.0003	0.0003	0.0004
error 0.2 mm	0.0006	0.0006	0.0006	0.0006	0.0007	0.0007	0.0007	0.0009
error 0.3 mm	0.0009	0.0010	0.0010	0.0010	0.0010	0.0011	0.0012	0.0015
error 0.4 mm	0.0013	0.0013	0.0013	0.0013	0.0014	0.0015	0.0017	0.0024
error 0.5 mm	0.0016	0.0016	0.0016	0.0017	0.0018	0.0019	0.0023	0.0034
error 0.6 mm	0.0019	0.0019	0.0020	0.0020	0.0022	0.0024	0.0030	0.0046
error 0.7 mm	0.0022	0.0023	0.0023	0.0024	0.0026	0.0029	0.0038	0.0061
error 0.8 mm	0.0026	0.0026	0.0027	0.0028	0.0030	0.0035	0.0047	0.0079
error 0.9 mm	0.0029	0.0029	0.0030	0.0032	0.0035	0.0041	0.0056	0.0100
error 1.0 mm	0.0032	0.0033	0.0034	0.0036	0.0039	0.0047	0.0066	0.0123

Table A.4: Data for comparing blur at different throughputs (5.6-degree maximum collection angle)

Length total	5000	5000	5000	5000	5000	5000	5000	5000
bc	7.02	7.02	7.02	7.02	7.02	7.02	7.02	7.02
Wmag	12	12	12	12	12	12	12	12
Theta_cf	3	3	3	3	3	3	3	3
delta_c	0.003286	0.006576	0.01317	0.0264	0.05302	0.10701	0.21812	0.45485
solid angle	0.000003	0.000006	0.000012	0.000024	0.000048	0.000096	0.000192	0.000384
refl angle	0.745183436	0.747385	0.751788	0.76058	0.7781	0.812934	0.881685	1.015063
length CD	3.12984829	6.257401	12.50774	24.9797	49.83037	99.48427	200.423	424.3466
dia CD	40.21895465	40.17483	40.08639	39.90895	39.55192	38.82778	37.33743	34.16176
error 0 mm	0.0000	0.0000	0.0000	0.0000	0.0000	0.0000	0.0000	0.0000
error 0.1 mm	0.0001	0.0001	0.0001	0.0001	0.0001	0.0002	0.0005	0.0013
error 0.2 mm	0.0002	0.0002	0.0002	0.0003	0.0004	0.0008	0.0018	0.0051
error 0.3 mm	0.0003	0.0003	0.0004	0.0005	0.0008	0.0018	0.0041	0.0114
error 0.4 mm	0.0004	0.0005	0.0006	0.0008	0.0015	0.0031	0.0072	0.0202
error 0.5 mm	0.0005	0.0006	0.0008	0.0012	0.0023	0.0049	0.0113	0.0316
error 0.6 mm	0.0007	0.0008	0.0010	0.0016	0.0033	0.0071	0.0163	0.0455
error 0.7 mm	0.0008	0.0009	0.0013	0.0022	0.0045	0.0096	0.0222	0.0619
error 0.8 mm	0.0009	0.0011	0.0016	0.0029	0.0059	0.0126	0.0290	0.0807
error 0.9 mm	0.0011	0.0013	0.0020	0.0036	0.0074	0.0159	0.0366	0.1021
error 1.0 mm	0.0012	0.0016	0.0024	0.0045	0.0092	0.0196	0.0452	0.1260

Table A.5: Data for comparing blur at different throughputs (3.0-degree maximum collection angle)

APPENDIX B: REFLECTIVITY DATA

Tables B.1 and B.2 contain the reflectivity data used in Figure 7.2.

reflection angle	ratio for 1 layer	ratio for 4 layers	ratio for 7 layers	ratio for 10 layers	ratio for 15 layers	ratio for 20 layers	ratio for 30 layers	ratio for 50 layers
1.300	0.0075	0.0265	0.0009	0.0264	0.0119	0.0011	0.0189	0.0145
1.304	0.0074	0.0278	0.0005	0.0268	0.0088	0.0023	0.0172	0.0110
1.308	0.0073	0.0292	0.0002	0.0268	0.0059	0.0050	0.0134	0.0059
1.312	0.0073	0.0305	0.0002	0.0264	0.0036	0.0087	0.0088	0.0037
1.316	0.0072	0.0318	0.0005	0.0255	0.0017	0.0133	0.0044	0.0064
1.320	0.0071	0.0331	0.0011	0.0242	0.0008	0.0181	0.0021	0.0125
1.324	0.0070	0.0344	0.0019	0.0225	0.0009	0.0226	0.0028	0.0174
1.328	0.0070	0.0357	0.0031	0.0204	0.0021	0.0260	0.0066	0.0173
1.332	0.0069	0.0370	0.0046	0.0181	0.0045	0.0281	0.0125	0.0122
1.336	0.0068	0.0383	0.0066	0.0155	0.0081	0.0285	0.0193	0.0061
1.340	0.0067	0.0395	0.0088	0.0129	0.0124	0.0270	0.0246	0.0046
1.344	0.0067	0.0408	0.0114	0.0102	0.0176	0.0238	0.0271	0.0097
1.348	0.0066	0.0420	0.0143	0.0076	0.0229	0.0194	0.0260	0.0177
1.352	0.0065	0.0432	0.0176	0.0052	0.0284	0.0141	0.0214	0.0230
1.356	0.0065	0.0443	0.0210	0.0032	0.0334	0.0090	0.0148	0.0213
1.360	0.0064	0.0454	0.0250	0.0016	0.0378	0.0046	0.0080	0.0137
1.364	0.0063	0.0465	0.0292	0.0007	0.0412	0.0019	0.0035	0.0065
1.368	0.0063	0.0476	0.0336	0.0005	0.0433	0.0017	0.0033	0.0066
1.372	0.0062	0.0486	0.0383	0.0012	0.0440	0.0044	0.0083	0.0153
1.376	0.0061	0.0495	0.0432	0.0029	0.0430	0.0099	0.0175	0.0266
1.380	0.0061	0.0505	0.0483	0.0056	0.0405	0.0179	0.0287	0.0321
1.384	0.0060	0.0514	0.0535	0.0095	0.0365	0.0277	0.0389	0.0275
1.388	0.0059	0.0522	0.0590	0.0148	0.0310	0.0385	0.0453	0.0157
1.392	0.0059	0.0530	0.0643	0.0211	0.0248	0.0484	0.0457	0.0076
1.396	0.0058	0.0538	0.0699	0.0288	0.0180	0.0569	0.0397	0.0118
1.400	0.0057	0.0545	0.0754	0.0374	0.0116	0.0623	0.0291	0.0273
1.404	0.0057	0.0552	0.0809	0.0471	0.0061	0.0643	0.0167	0.0437
1.408	0.0056	0.0558	0.0864	0.0580	0.0024	0.0622	0.0070	0.0485
1.412	0.0056	0.0564	0.0917	0.0693	0.0016	0.0562	0.0051	0.0377
1.416	0.0055	0.0569	0.0970	0.0817	0.0044	0.0464	0.0140	0.0191
1.420	0.0055	0.0574	0.1022	0.0945	0.0117	0.0339	0.0335	0.0110
1.424	0.0054	0.0578	0.1072	0.1077	0.0240	0.0208	0.0595	0.0267
1.428	0.0053	0.0582	0.1120	0.1211	0.0414	0.0096	0.0851	0.0586
1.432	0.0053	0.0585	0.1167	0.1348	0.0647	0.0038	0.1040	0.0840
1.436	0.0052	0.0588	0.1211	0.1479	0.0915	0.0075	0.1096	0.0818
1.440	0.0052	0.0590	0.1251	0.1607	0.1217	0.0236	0.0999	0.0528
1.444	0.0051	0.0592	0.1291	0.1735	0.1553	0.0551	0.0744	0.0220
1.448	0.0051	0.0593	0.1326	0.1852	0.1887	0.0991	0.0414	0.0353
1.452	0.0050	0.0594	0.1359	0.1966	0.2233	0.1555	0.0152	0.1046
1.456	0.0049	0.0594	0.1389	0.2072	0.2566	0.2180	0.0247	0.1782
1.460	0.0049	0.0594	0.1415	0.2169	0.2879	0.2813	0.0935	0.1966
1.464	0.0048	0.0593	0.1438	0.2256	0.3165	0.3410	0.2150	0.1334
1.468	0.0048	0.0592	0.1458	0.2331	0.3413	0.3925	0.3484	0.0589
1.472	0.0047	0.0590	0.1474	0.2401	0.3643	0.4395	0.4733	0.2300
1.476	0.0047	0.0588	0.1487	0.2458	0.3832	0.4767	0.5631	0.5256
1.480	0.0046	0.0586	0.1496	0.2504	0.3986	0.5059	0.6239	0.6849
1.484	0.0046	0.0583	0.1502	0.2541	0.4109	0.5281	0.6628	0.7484
1.488	0.0045	0.0579	0.1505	0.2567	0.4203	0.5443	0.6861	0.7710
1.492	0.0045	0.0575	0.1504	0.2582	0.4263	0.5541	0.6971	0.7748
1.496	0.0044	0.0570	0.1499	0.2587	0.4296	0.5591	0.6998	0.7694
1.500	0.0044	0.0566	0.1492	0.2583	0.4300	0.5593	0.6961	0.7587
1.504	0.0043	0.0560	0.1481	0.2567	0.4276	0.5552	0.6867	0.7433
1.508	0.0043	0.0555	0.1467	0.2542	0.4227	0.5471	0.6724	0.7237
1.512	0.0043	0.0549	0.1450	0.2509	0.4155	0.5355	0.6541	0.7006
1.516	0.0042	0.0543	0.1430	0.2466	0.4057	0.5198	0.6301	0.6713
1.520	0.0042	0.0536	0.1407	0.2414	0.3935	0.5003	0.6004	0.6346
1.524	0.0041	0.0528	0.1380	0.2351	0.3785	0.4761	0.5630	0.5861
1.528	0.0041	0.0521	0.1352	0.2282	0.3618	0.4488	0.5189	0.5242
1.532	0.0040	0.0514	0.1321	0.2207	0.3431	0.4176	0.4659	0.4417
1.536	0.0040	0.0506	0.1288	0.2124	0.3224	0.3824	0.4028	0.3346
1.540	0.0039	0.0497	0.1252	0.2033	0.2991	0.3423	0.3272	0.2106

Table B.1: Reflectivity data (continued in Table B.2)

reflection angle	ratio for 1 layer	ratio for 4 layers	ratio for 7 layers	ratio for 10 layers	ratio for 15 layers	ratio for 20 layers	ratio for 30 layers	ratio for 50 layers
1.544	0.0039	0.0489	0.1215	0.1938	0.2750	0.3002	0.2464	0.1230
1.548	0.0039	0.0480	0.1175	0.1836	0.2488	0.2543	0.1625	0.1052
1.552	0.0038	0.0471	0.1133	0.1729	0.2216	0.2071	0.0899	0.1207
1.556	0.0038	0.0462	0.1091	0.1623	0.1948	0.1619	0.0425	0.1167
1.560	0.0037	0.0452	0.1047	0.1511	0.1670	0.1181	0.0226	0.0853
1.564	0.0037	0.0443	0.1002	0.1397	0.1398	0.0795	0.0267	0.0468
1.568	0.0037	0.0433	0.0956	0.1282	0.1138	0.0481	0.0424	0.0258
1.572	0.0036	0.0423	0.0910	0.1168	0.0895	0.0252	0.0580	0.0297
1.576	0.0036	0.0413	0.0863	0.1055	0.0677	0.0111	0.0667	0.0441
1.580	0.0035	0.0402	0.0814	0.0941	0.0482	0.0050	0.0661	0.0508
1.584	0.0035	0.0392	0.0767	0.0834	0.0326	0.0054	0.0573	0.0428
1.588	0.0035	0.0382	0.0721	0.0732	0.0203	0.0101	0.0435	0.0264
1.592	0.0034	0.0371	0.0673	0.0631	0.0110	0.0170	0.0277	0.0126
1.596	0.0034	0.0361	0.0627	0.0539	0.0052	0.0241	0.0145	0.0100
1.600	0.0033	0.0350	0.0582	0.0454	0.0022	0.0301	0.0064	0.0166
1.604	0.0033	0.0340	0.0537	0.0374	0.0014	0.0343	0.0040	0.0245
1.608	0.0033	0.0329	0.0494	0.0303	0.0025	0.0361	0.0067	0.0261
1.612	0.0032	0.0318	0.0451	0.0239	0.0049	0.0356	0.0125	0.0202
1.616	0.0032	0.0308	0.0411	0.0184	0.0080	0.0329	0.0185	0.0112
1.620	0.0032	0.0297	0.0372	0.0137	0.0113	0.0287	0.0228	0.0053
1.624	0.0031	0.0287	0.0334	0.0097	0.0145	0.0234	0.0241	0.0058
1.628	0.0031	0.0277	0.0299	0.0066	0.0173	0.0177	0.0222	0.0106
1.632	0.0031	0.0267	0.0266	0.0041	0.0195	0.0123	0.0179	0.0150
1.636	0.0030	0.0256	0.0234	0.0023	0.0209	0.0074	0.0123	0.0153
1.640	0.0030	0.0246	0.0205	0.0011	0.0215	0.0039	0.0070	0.0113
1.644	0.0030	0.0236	0.0177	0.0005	0.0213	0.0016	0.0031	0.0058
1.648	0.0029	0.0226	0.0152	0.0003	0.0203	0.0008	0.0015	0.0028
1.652	0.0029	0.0217	0.0129	0.0004	0.0188	0.0012	0.0021	0.0038
1.656	0.0029	0.0207	0.0108	0.0009	0.0167	0.0026	0.0044	0.0073
1.660	0.0028	0.0198	0.0089	0.0016	0.0143	0.0045	0.0074	0.0100
1.664	0.0028	0.0188	0.0072	0.0025	0.0118	0.0067	0.0100	0.0098
1.668	0.0028	0.0179	0.0058	0.0034	0.0093	0.0088	0.0114	0.0069
1.672	0.0027	0.0171	0.0045	0.0044	0.0069	0.0104	0.0114	0.0034
1.676	0.0027	0.0162	0.0034	0.0054	0.0048	0.0114	0.0099	0.0018
1.680	0.0027	0.0153	0.0025	0.0064	0.0030	0.0116	0.0074	0.0028
1.684	0.0026	0.0145	0.0017	0.0072	0.0016	0.0112	0.0047	0.0052
1.688	0.0026	0.0137	0.0012	0.0080	0.0008	0.0101	0.0024	0.0070
1.692	0.0026	0.0130	0.0007	0.0086	0.0003	0.0085	0.0010	0.0067
1.696	0.0026	0.0122	0.0004	0.0090	0.0003	0.0067	0.0008	0.0046
1.700	0.0025	0.0115	0.0002	0.0093	0.0006	0.0048	0.0016	0.0022

Table B.2: Reflectivity data (continuation of Table B.1)

APPENDIX C: MOST PROMISING DESIGN – GEOMETRIC PARAMETERS

The most promising design uses the geometric parameters given here[1]. The hyperbola and ellipse parameters for the mirrors are given on the next page.

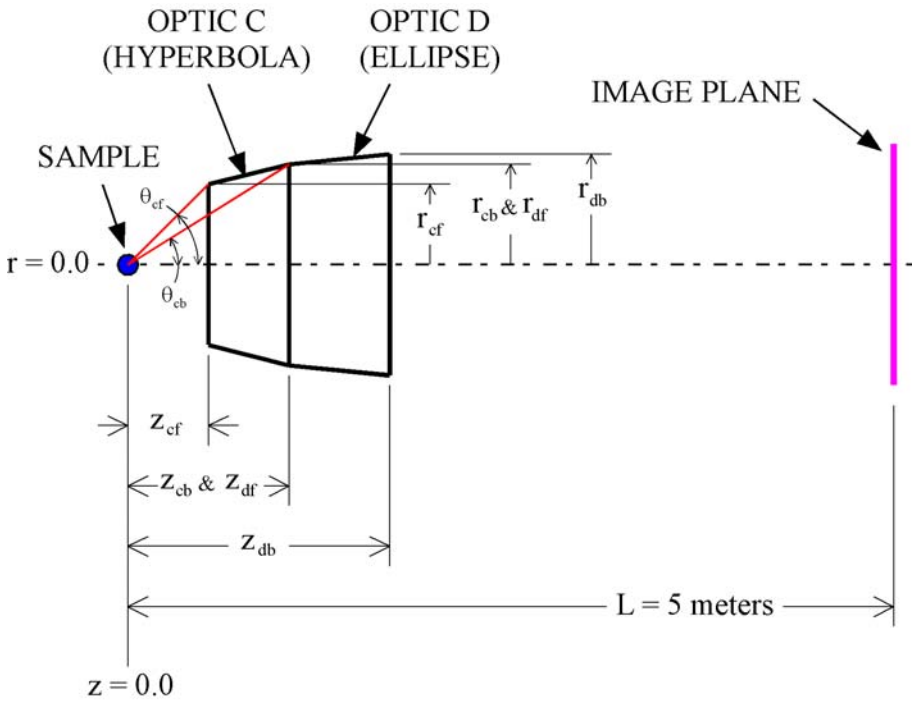

Figure C.1: Geometric parameters

Sample Location:

z_{sample} = 0.0 mm $\quad$ r_{sample} = 0.0 mm

Optic C:

Z_{cf} =	340.752820 mm	r_{cf} =	33.411106 mm	θ_{cf} =	5.6000000 degrees
Z_{cb} =	383.037896 mm	r_{cb} =	36.349392 mm	θ_{cb} =	5.4210000 degrees

Optic D:

Z_{df} =	383.037896 mm	r_{df} =	36.349392 mm
Z_{db} =	430.301983 mm	r_{db} =	37.167143 mm

Image Plane:

Z_{image} = 5000.0 mm

[1] NOTE: some of the geometric parameters shown here are no longer being used. They have been revised because of manufacturing limitations. The optics have been slightly shortened, but the hyperbola/ellipse intersection parameters and the hyperbola and ellipse parameters (next page) remain unchanged. The revised parameters are given in Appendix G.

Hyperbola Parameters (optic C):

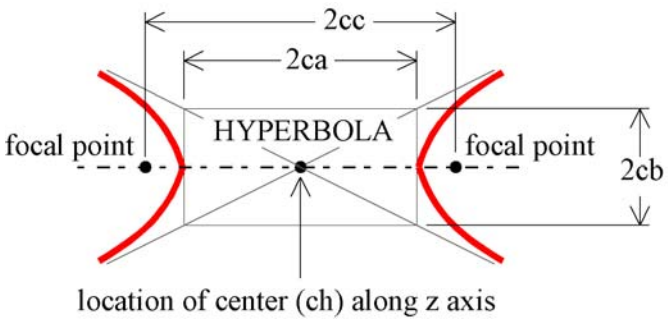

Major axis length (ca) =	227.440417451930 mm
Minor axis length (cb) =	14.580000000000 mm
Focal length (cc) =	227.907261601530 mm
Center location (ch) =	-227.907261601530 mm

Ellipse Parameters (optic D):

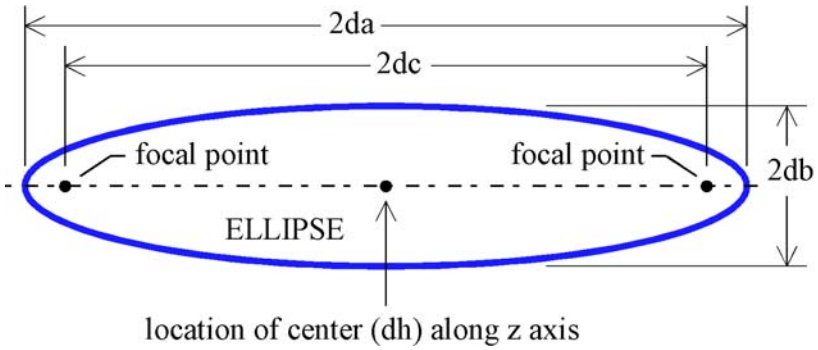

Major axis length (da) =	2728.372396151007 mm
Minor axis length (db) =	50.377615866900 mm
Focal length (dc) =	2727.907261601530 mm
Center location (dh) =	2272.092738398470 mm

Determination of the geometric parameters:

Only five parameters are needed to describe the system; the remaining parameters can be determined from the original five. The five parameters that we are using to fix or design are given in Table C-1.

Parameter	Description
L	Distance from the object plane to the image plane
wmag	System magnification
cb	Hyperbola (optic C) minor axis
θ_{cf}	Angle – target to front of optic C
$\Delta\theta_c$	Angle – difference between θ_{cf} and θ_{cb}

Table C-1: five parameters are used to describe the optical system

A nomenclature is used when naming the parameters. If the parameter is describing an angle, then one of the following characters will be used: θ, α, β, or γ. If the parameter describes the difference between two other parameters, then we will use a Δ to represent the difference. If a parameter is associated with optic C (the hyperbola), then it will have the letter "c" in its name. If a parameter is associated with optic D (the ellipse), then it will have the letter "d" in its name. The optic letter can be followed by an "f" for front or a "b" for back. The front of an optic is the side closest to the object plane. The back of an optic is the side closest to the image plane (see Figure C-1 for some examples). An "i" is used to indicate the point of intersection between optic C and optic D.

The calculations required for finding the remainder of the system parameters are described below. Equation 1 calculates the angle from the object center to the back of optic C (see Figure C-2). Equation 2 shows the equation for calculating the magnification (see Figure C-3). Equation 3 rewrites equation 2 to determine θ_{df}.

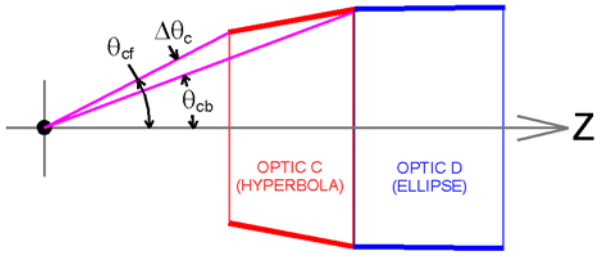

Figure C-2: important angles

$$\theta_{cb} = \theta_{cf} - \Delta\theta_c \qquad \text{(eq 1)}$$

$$\text{wmag} = \frac{\sin(\theta_{cb})}{\sin(\theta_{df})} \qquad \text{(eq 2)}$$

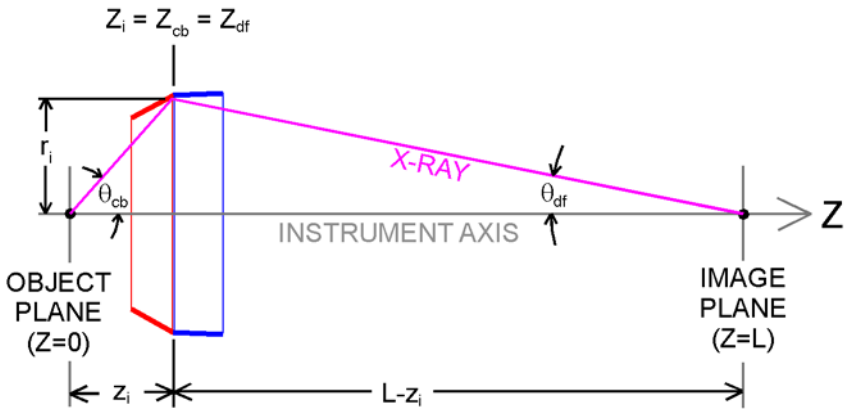

Figure C-3: important parameters

$$\theta_{df} = \sin^{-1}\left(\frac{\sin(\theta_{cb})}{wmag}\right) \qquad \text{(eq 3)}$$

The intersection point between optic C and optic D is calculated next (see Figure C-3). Using trigonometry, we can create two equations (equations 4 and 5). These equations can be re-arranged (equations 6 and 7) and combined into one equation (equation 8). Equation 8 can be solved for the z value of the intersection (equation 9). With the z value known, the radius at the intersection can be calculated (equation 6).

$$\tan(\theta_{cb}) = r_i / z_i \qquad \text{(eq 4)}$$

$$\tan(\theta_{df}) = r_i / (L - z_i) \qquad \text{(eq 5)}$$

$$r_i = z_i \tan(\theta_{cb}) \qquad \text{(eq 6)}$$

$$r_i = (L - z_i)\tan(\theta_{df}) \qquad \text{(eq 7)}$$

$$z_i \tan(\theta_{cb}) = (L - z_i)\tan(\theta_{df}) \qquad \text{(eq 8)}$$

$$z_i = \frac{L \tan(\theta_{df})}{\tan(\theta_{cb}) + \tan(\theta_{df})} \qquad \text{(eq 9)}$$

The hyperboloid parameters are calculated next. Equations 10, 11, and 12 represent a system of equations that must be solved to find ca, cb, and ch. Figure C-4 shows the hyperboloid and its parameters. With the hyperboloid parameters known, the center of the ellipsoid (dh) and the focal length of the ellipsoid (dc) can be calculated (see equations 13 and 14). The remaining ellipsoid parameters (da and db) are found by solving a system of equations (see equations 15 and 16). Figure C-5 shows the ellipsoid and its parameters.

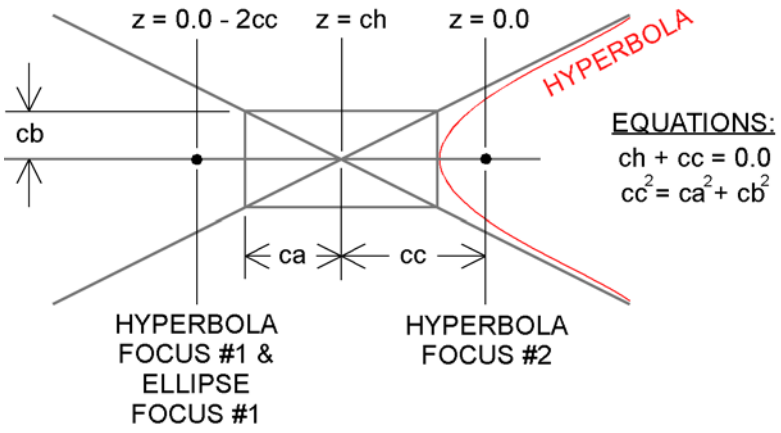

Figure C-4: Hyperboloid (optic C) parameters

$$(cb)^2(z-ch)^2-(ca)^2r^2=(ca)^2(cb)^2 \quad \text{(eq 10)}$$

$$(ch)+(cc)=0 \quad \text{(eq 11)}$$

$$(cc)^2=(ca)^2+(cb)^2 \quad \text{(eq 12)}$$

$$(dh)=(L-2(cc))/2 \quad \text{(eq 13)}$$

$$(dc)=(L+2(cc))/2 \quad \text{(eq 14)}$$

$$(db)^2(z-dh)^2+(da)^2r^2=(da)^2(db)^2 \quad \text{(eq 15)}$$

$$(dc)^2=(da)^2-(db)^2 \quad \text{(eq 16)}$$

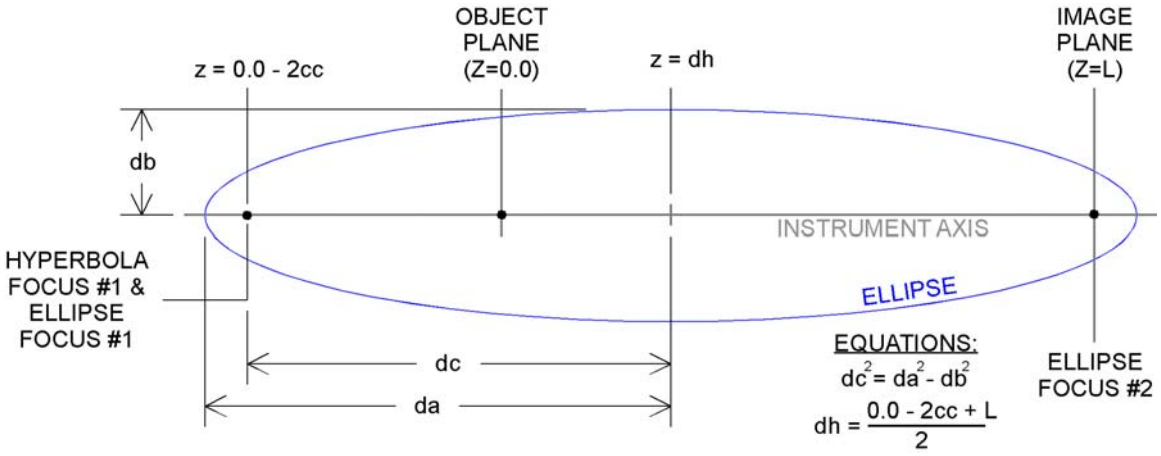

Figure C-5: Ellipsoid (optic D) parameters

The next step is finding the front point of optic C, (z_{cf}, r_{cf}). Finding the intersection of a line and the hyperboloid accomplishes this task. Equation 17 represents the hyperboloid, and equation 18 represents the line. This system of equations must be solved to find the unknowns. Figure C-6 shows the intersection that we are trying to find. We now have enough information to calculate the length of optic C (equation 19).

$$(cb)^2(z_{cf} - ch)^2 - (ca)^2 r_{cf}^2 = (ca)^2(cb)^2 \qquad \text{(eq 17)}$$

$$r_{cf} = mz_{cf} + b \quad \text{where} \quad m = \tan(\theta_{cf}) \quad \text{and} \quad b = 0 \qquad \text{(eq 18)}$$

$$L_c = z_{cb} - z_{cf} \qquad \text{(eq 19)}$$

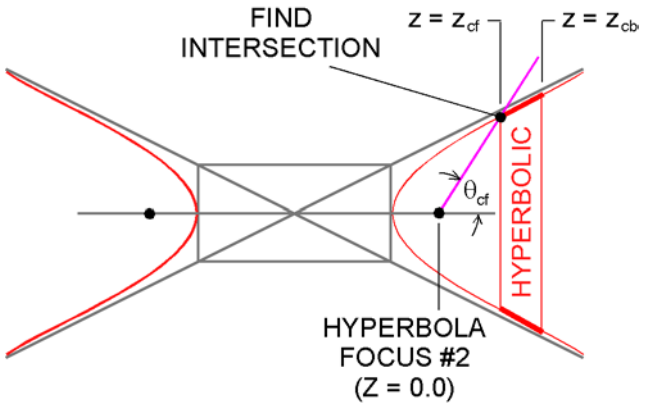

Figure C-6: Finding the front point of optic C

Now we will find the back point of optic D, (z_{db}, r_{db}). Similar to the last step, finding the intersection of a line and the ellipse accomplishes this task. We first need to calculate a useful number, tanγ (see Figure C-7 and equation 20). Equation 21 represents the ellipse, and equation 22 represents the line. This system of equations must be solved to find the unknowns.

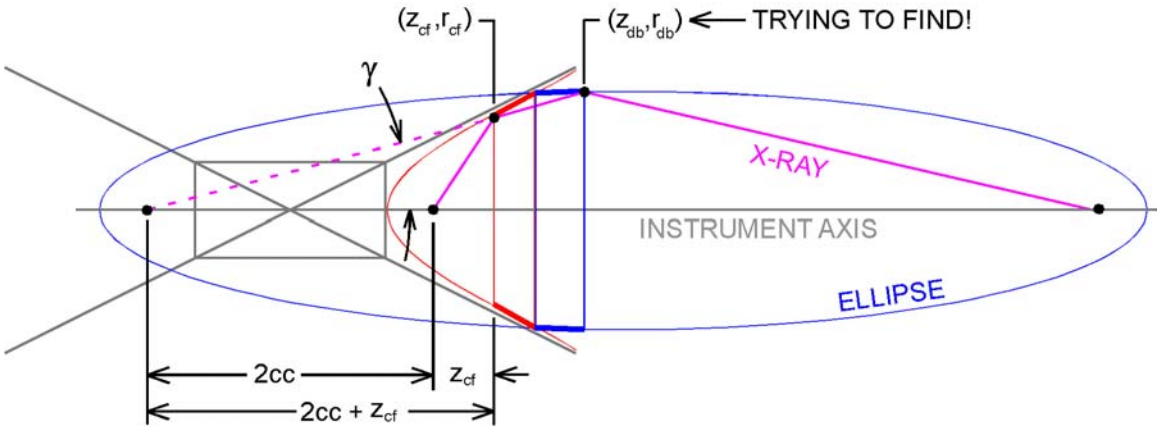

Figure C-7: Finding the back point of optic D

$$\tan\gamma = \frac{r_{cf}}{z_{cf} + 2(cc)} \qquad \text{(eq 20)}$$

$$(db)^2(z_{db} - dh)^2 + (da)^2 r_{db}^2 = (da)^2(db)^2 \qquad \text{(eq 21)}$$

$$r_{db} = mz_{db} + b \quad \text{where} \quad m = \tan\gamma \quad \text{and} \quad b = 2(cc)\tan\gamma \qquad \text{(eq 22)}$$

During the optical design process, we need to know what the reflection angles will be at the optical extremes (front and back of both optics). Too large or small of a reflection angle can ruin the design. Figure C-8 shows the relationship between various angles and the reflection angle for optic C. We need to know the slope at the front and rear of optic C to find the reflection angles. Equation 23 is the equation for the hyperbola. Equation 24 is the derivative of equation 23. Equation 25 shows the slope of the hyperbola in general. It can be used to find the slope at any point along optic C. With the slope known, the reflection angles at the front and rear of optic C can be calculated (equations 26 and 27).

$$(cb)^2(z-ch)^2-(ca)^2r^2=(ca)^2(cb)^2 \qquad \text{(eq 23)}$$

$$2(cb)^2(z-ch)dz-2(ca)^2rdr=0 \qquad \text{(eq 24)}$$

$$\frac{dr}{dz}=\frac{(cb)^2(z-ch)}{(ca)^2r} \qquad \text{(eq 25)}$$

$$\alpha_{cf}=\theta_{cf}-\tan^{-1}\left(\frac{dr}{dz}\Big|_{cf}\right) \qquad \text{(eq 26)}$$

$$\alpha_{cb}=\theta_{cb}-\tan^{-1}\left(\frac{dr}{dz}\Big|_{cb}\right) \qquad \text{(eq 27)}$$

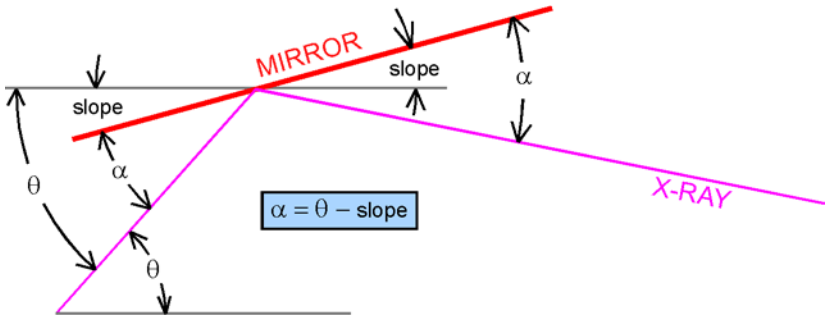

Figure C-8: Angle relationships for optic C

Figure C-9 shows the relationship between various angles and the reflection angle for optic D. We need to know the slope at the front and rear of optic D to find the reflection angles. Equation 28 is the equation for the ellipse. Equation 29 is the derivative of equation 28. Equation 30 shows the slope of the ellipse in general. It can be used to find the slope at any point along optic D. With the slope known, the reflection angles at the front and rear of optic D can be calculated (equations 31 and 32).

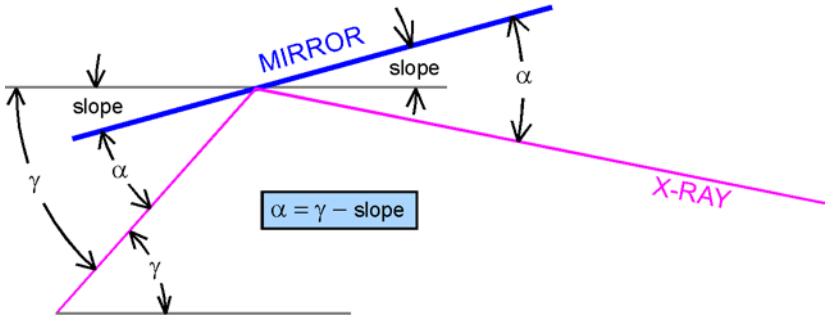

Figure C-9: Angle relationships for optic D

$$(db)^2(z-dh)^2+(da)^2r^2=(da)^2(db)^2 \qquad \text{(eq 28)}$$

$$2(db)^2(z-dh)dz+2(da)^2rdr=0 \qquad \text{(eq 29)}$$

$$\frac{dr}{dz}=\frac{-(db)^2(z-dh)}{(da)^2r} \qquad \text{(eq 30)}$$

$$\alpha_{df}=\theta_{df}-\tan^{-1}\left(\frac{dr}{dz}\Big|_{df}\right) \qquad \text{(eq 31)}$$

$$\alpha_{db}=\theta_{db}-\tan^{-1}\left(\frac{dr}{dz}\Big|_{db}\right) \qquad \text{(eq 32)}$$

APPENDIX D: MOST PROMISING DESIGN – MIRROR REFLECTION ANGLES

This appendix contains the middle reflection angle versus z-axis position for both mirrors. Maximum reflection angle range for this design is also given. Figures D.1 and D.2 illustrate the reflection data that is given in Tables D.1 and D.2.

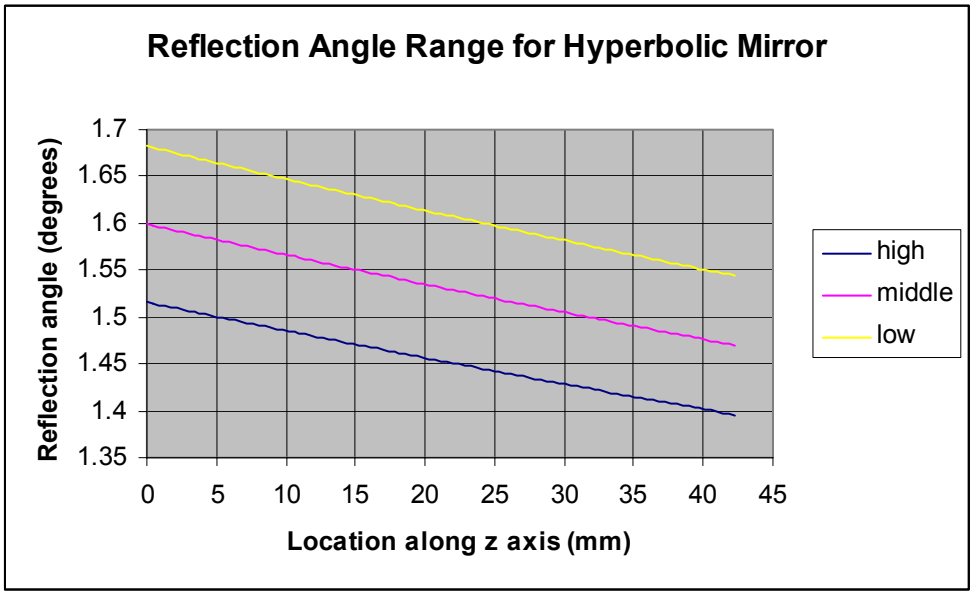

Figure D.1: Reflection angle data (maximum, minimum, and nominal) for the hyperbolic mirror
Middle line equation: y = (-0.0030507)z+2.6364

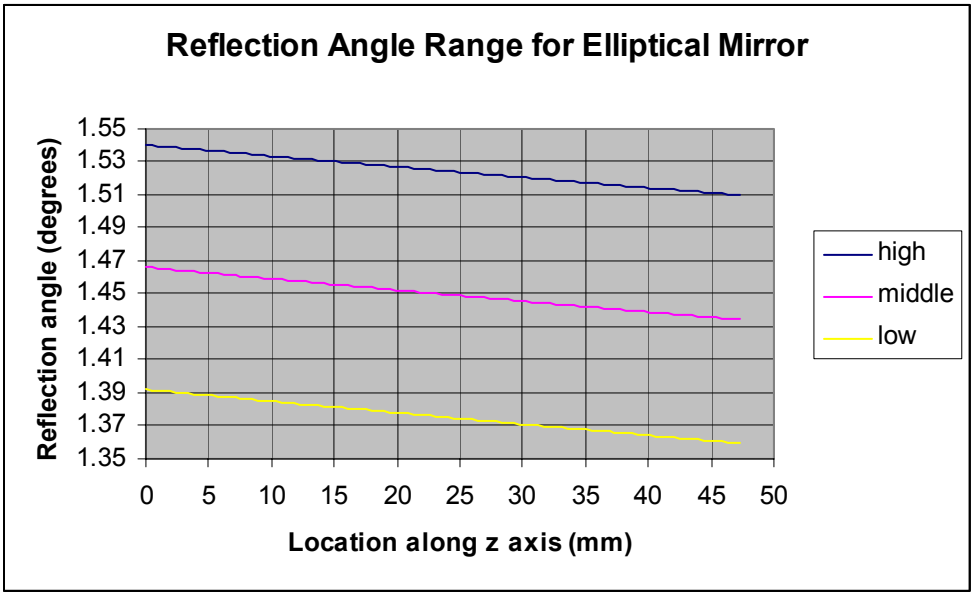

Figure D.2: Reflection angle data (maximum, minimum, and nominal) for the elliptical mirror
Middle line equation: y = (-0.000673)z+1.7236

Mirror C - Hyperbola					Mirror D - Ellipse				
Z location	Z_loc_C	low angle	mid angle	high angle	Z location	Z_loc_C	low angle	mid angle	high angle
340.753	0	1.5158	1.5991	1.6824	383.038	0	1.392	1.4661	1.5403
341.176	0.423	1.5145	1.5977	1.6808	383.511	0.473	1.3917	1.4658	1.54
341.599	0.846	1.5132	1.5963	1.6793	383.983	0.945	1.3913	1.4655	1.5396
342.021	1.268	1.5119	1.5949	1.6778	384.456	1.418	1.391	1.4651	1.5393
342.444	1.691	1.5106	1.5935	1.6763	384.928	1.89	1.3907	1.4648	1.539
342.867	2.114	1.5093	1.5921	1.6748	385.401	2.363	1.3903	1.4645	1.5387
343.29	2.537	1.508	1.5907	1.6733	385.874	2.836	1.39	1.4642	1.5384
343.713	2.96	1.5067	1.5893	1.6718	386.346	3.308	1.3897	1.4638	1.538
344.136	3.383	1.5054	1.5879	1.6703	386.819	3.781	1.3893	1.4635	1.5377
344.558	3.805	1.5041	1.5865	1.6688	387.292	4.254	1.389	1.4632	1.5374
344.981	4.228	1.5028	1.5851	1.6673	387.764	4.726	1.3886	1.4628	1.5371
345.404	4.651	1.5015	1.5837	1.6658	388.237	5.199	1.3883	1.4625	1.5368
345.827	5.074	1.5002	1.5823	1.6644	388.71	5.672	1.388	1.4622	1.5365
346.25	5.497	1.499	1.5809	1.6629	389.182	6.144	1.3876	1.4618	1.5361
346.673	5.92	1.4977	1.5796	1.6614	389.655	6.617	1.3873	1.4615	1.5358
347.096	6.343	1.4964	1.5782	1.6599	390.128	7.09	1.387	1.4612	1.5355
347.518	6.765	1.4951	1.5768	1.6585	390.6	7.562	1.3866	1.4608	1.5352
347.941	7.188	1.4939	1.5754	1.657	391.073	8.035	1.3863	1.4605	1.5349
348.364	7.611	1.4926	1.5741	1.6555	391.545	8.507	1.386	1.4602	1.5346
348.787	8.034	1.4913	1.5727	1.6541	392.018	8.98	1.3856	1.4599	1.5343
349.21	8.457	1.4901	1.5713	1.6526	392.491	9.453	1.3853	1.4595	1.5339
349.633	8.88	1.4888	1.57	1.6511	392.963	9.925	1.385	1.4592	1.5336
350.056	9.303	1.4875	1.5686	1.6497	393.436	10.398	1.3846	1.4589	1.5333
350.478	9.725	1.4863	1.5673	1.6482	393.909	10.871	1.3843	1.4586	1.533
350.901	10.148	1.485	1.5659	1.6468	394.381	11.343	1.384	1.4582	1.5327
351.324	10.571	1.4838	1.5646	1.6453	394.854	11.816	1.3836	1.4579	1.5324
351.747	10.994	1.4825	1.5632	1.6439	395.327	12.289	1.3833	1.4576	1.5321
352.17	11.417	1.4813	1.5619	1.6424	395.799	12.761	1.383	1.4573	1.5318
352.593	11.84	1.48	1.5605	1.641	396.272	13.234	1.3826	1.4569	1.5314
353.015	12.262	1.4788	1.5592	1.6396	396.744	13.706	1.3823	1.4566	1.5311
353.438	12.685	1.4775	1.5578	1.6381	397.217	14.179	1.382	1.4563	1.5308
353.861	13.108	1.4763	1.5565	1.6367	397.69	14.652	1.3816	1.456	1.5305
354.284	13.531	1.475	1.5552	1.6353	398.162	15.124	1.3813	1.4556	1.5302
354.707	13.954	1.4738	1.5538	1.6338	398.635	15.597	1.381	1.4553	1.5299
355.13	14.377	1.4726	1.5525	1.6324	399.108	16.07	1.3806	1.455	1.5296
355.553	14.8	1.4713	1.5512	1.631	399.58	16.542	1.3803	1.4547	1.5293
355.975	15.222	1.4701	1.5499	1.6296	400.053	17.015	1.38	1.4543	1.529
356.398	15.645	1.4689	1.5485	1.6282	400.526	17.488	1.3797	1.454	1.5287
356.821	16.068	1.4677	1.5472	1.6267	400.998	17.96	1.3793	1.4537	1.5284
357.244	16.491	1.4664	1.5459	1.6253	401.471	18.433	1.379	1.4534	1.528
357.667	16.914	1.4652	1.5446	1.6239	401.944	18.906	1.3787	1.4531	1.5277
358.09	17.337	1.464	1.5433	1.6225	402.416	19.378	1.3783	1.4527	1.5274
358.513	17.76	1.4628	1.542	1.6211	402.889	19.851	1.378	1.4524	1.5271
358.935	18.182	1.4616	1.5407	1.6197	403.361	20.323	1.3777	1.4521	1.5268
359.358	18.605	1.4604	1.5394	1.6183	403.834	20.796	1.3774	1.4518	1.5265
359.781	19.028	1.4592	1.538	1.6169	404.307	21.269	1.377	1.4515	1.5262
360.204	19.451	1.4579	1.5367	1.6155	404.779	21.741	1.3767	1.4511	1.5259
360.627	19.874	1.4567	1.5355	1.6142	405.252	22.214	1.3764	1.4508	1.5256
361.05	20.297	1.4555	1.5342	1.6128	405.725	22.687	1.3761	1.4505	1.5253
361.473	20.72	1.4543	1.5329	1.6114	406.197	23.159	1.3757	1.4502	1.525
361.895	21.142	1.4531	1.5316	1.61	406.67	23.632	1.3754	1.4499	1.5247
362.318	21.565	1.4519	1.5303	1.6086	407.143	24.105	1.3751	1.4495	1.5244
362.741	21.988	1.4507	1.529	1.6072	407.615	24.577	1.3748	1.4492	1.5241
363.164	22.411	1.4495	1.5277	1.6059	408.088	25.05	1.3744	1.4489	1.5238
363.587	22.834	1.4484	1.5264	1.6045	408.561	25.523	1.3741	1.4486	1.5235
364.01	23.257	1.4472	1.5252	1.6031	409.033	25.995	1.3738	1.4483	1.5232
364.432	23.679	1.446	1.5239	1.6018	409.506	26.468	1.3735	1.448	1.5229
364.855	24.102	1.4448	1.5226	1.6004	409.978	26.94	1.3731	1.4476	1.5226
365.278	24.525	1.4436	1.5213	1.599	410.451	27.413	1.3728	1.4473	1.5223
365.701	24.948	1.4424	1.5201	1.5977	410.924	27.886	1.3725	1.447	1.522
366.124	25.371	1.4413	1.5188	1.5963	411.396	28.358	1.3722	1.4467	1.5217
366.547	25.794	1.4401	1.5175	1.595	411.869	28.831	1.3719	1.4464	1.5214
366.97	26.217	1.4389	1.5163	1.5936	412.342	29.304	1.3715	1.4461	1.5211
367.392	26.639	1.4377	1.515	1.5923	412.814	29.776	1.3712	1.4457	1.5208
367.815	27.062	1.4366	1.5137	1.5909	413.287	30.249	1.3709	1.4454	1.5205
368.238	27.485	1.4354	1.5125	1.5896	413.76	30.722	1.3706	1.4451	1.5202
368.661	27.908	1.4342	1.5112	1.5882	414.232	31.194	1.3703	1.4448	1.5199
369.084	28.331	1.4331	1.51	1.5869	414.705	31.667	1.3699	1.4445	1.5196
369.507	28.754	1.4319	1.5087	1.5856	415.177	32.139	1.3696	1.4442	1.5193
369.93	29.177	1.4307	1.5075	1.5842	415.65	32.612	1.3693	1.4439	1.519
370.352	29.599	1.4296	1.5062	1.5829	416.123	33.085	1.369	1.4436	1.5187

Table D.1: Reflection angle data for both mirrors (continued in next table)

Mirror C - Hyperbola (Continued)						Mirror D - Ellipse (Continued)				
Z location	Z_loc_C	low angle	mid angle	high angle		Z location	Z_loc_C	low angle	mid angle	high angle
370.352	29.599	1.4296	1.5062	1.5829		416.123	33.085	1.369	1.4436	1.5187
370.775	30.022	1.4284	1.505	1.5816		416.595	33.557	1.3687	1.4432	1.5184
371.198	30.445	1.4273	1.5038	1.5802		417.068	34.03	1.3683	1.4429	1.5181
371.621	30.868	1.4261	1.5025	1.5789		417.541	34.503	1.368	1.4426	1.5178
372.044	31.291	1.425	1.5013	1.5776		418.013	34.975	1.3677	1.4423	1.5175
372.467	31.714	1.4238	1.5001	1.5763		418.486	35.448	1.3674	1.442	1.5172
372.889	32.136	1.4227	1.4988	1.5749		418.959	35.921	1.3671	1.4417	1.5169
373.312	32.559	1.4215	1.4976	1.5736		419.431	36.393	1.3668	1.4414	1.5166
373.735	32.982	1.4204	1.4964	1.5723		419.904	36.866	1.3664	1.4411	1.5163
374.158	33.405	1.4193	1.4951	1.571		420.377	37.339	1.3661	1.4408	1.516
374.581	33.828	1.4181	1.4939	1.5697		420.849	37.811	1.3658	1.4404	1.5157
375.004	34.251	1.417	1.4927	1.5684		421.322	38.284	1.3655	1.4401	1.5154
375.427	34.674	1.4159	1.4915	1.5671		421.794	38.756	1.3652	1.4398	1.5151
375.849	35.096	1.4147	1.4903	1.5658		422.267	39.229	1.3649	1.4395	1.5148
376.272	35.519	1.4136	1.489	1.5645		422.74	39.702	1.3645	1.4392	1.5145
376.695	35.942	1.4125	1.4878	1.5632		423.212	40.174	1.3642	1.4389	1.5142
377.118	36.365	1.4113	1.4866	1.5619		423.685	40.647	1.3639	1.4386	1.514
377.541	36.788	1.4102	1.4854	1.5606		424.158	41.12	1.3636	1.4383	1.5137
377.964	37.211	1.4091	1.4842	1.5593		424.63	41.592	1.3633	1.438	1.5134
378.387	37.634	1.408	1.483	1.558		425.103	42.065	1.363	1.4377	1.5131
378.809	38.056	1.4068	1.4818	1.5567		425.576	42.538	1.3627	1.4374	1.5128
379.232	38.479	1.4057	1.4806	1.5555		426.048	43.01	1.3623	1.4371	1.5125
379.655	38.902	1.4046	1.4794	1.5542		426.521	43.483	1.362	1.4368	1.5122
380.078	39.325	1.4035	1.4782	1.5529		426.993	43.955	1.3617	1.4365	1.5119
380.501	39.748	1.4024	1.477	1.5516		427.466	44.428	1.3614	1.4361	1.5116
380.924	40.171	1.4013	1.4758	1.5503		427.939	44.901	1.3611	1.4358	1.5113
381.346	40.593	1.4002	1.4746	1.5491		428.411	45.373	1.3608	1.4355	1.511
381.769	41.016	1.3991	1.4734	1.5478		428.884	45.846	1.3605	1.4352	1.5108
382.192	41.439	1.398	1.4723	1.5465		429.357	46.319	1.3602	1.4349	1.5105
382.615	41.862	1.3969	1.4711	1.5453		429.829	46.791	1.3599	1.4346	1.5102
383.038	42.285	1.3958	1.4699	1.544		430.302	47.264	1.3595	1.4343	1.5099

Table D.2: Reflection angle data for both mirrors (continuation of previous table)

APPENDIX E: MOST PROMISING DESIGN – THEORETICAL INSTRUMENT RESOLUTION – SIMULATION DATA

Two different methods of looking at resolution are given here. One uses a line pair the other uses an edge. The line pair method tries to determine the minimum line spacing that can be seen at the detector (image plane). The line spacing changes depending on the off-axis position being studied (i.e., the y value in Figure E.1). Figure E.1 illustrates the method being used. Figure E.2 shows the theoretical resolution of the instrument using this method. The edge method creates intensity plots at different off-axis positions.

Resolution using line pair technique:

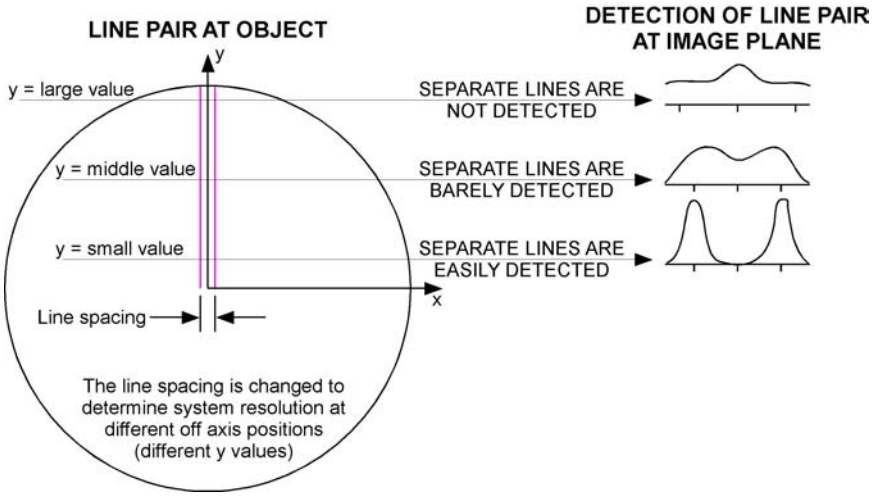

Figure E.1: Line pair resolution method

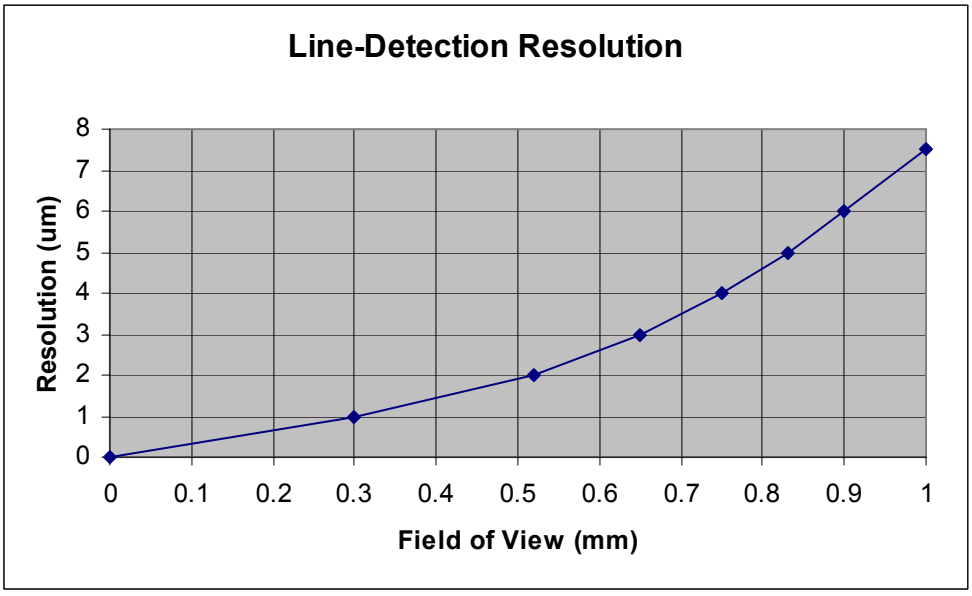

Figure E.2: Theoretical resolution of the most promising design using line pair method

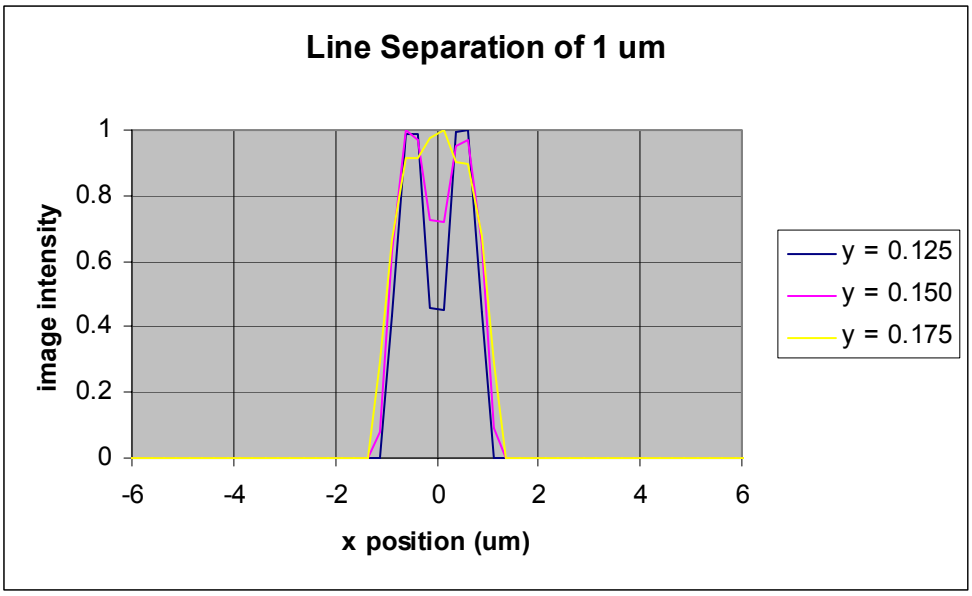

Figure E.3: Lines separated by 1 micrometer can be detected at an off-axis position of 0.150 millimeters (y=0.150 mm, FOV = 0.30 mm)

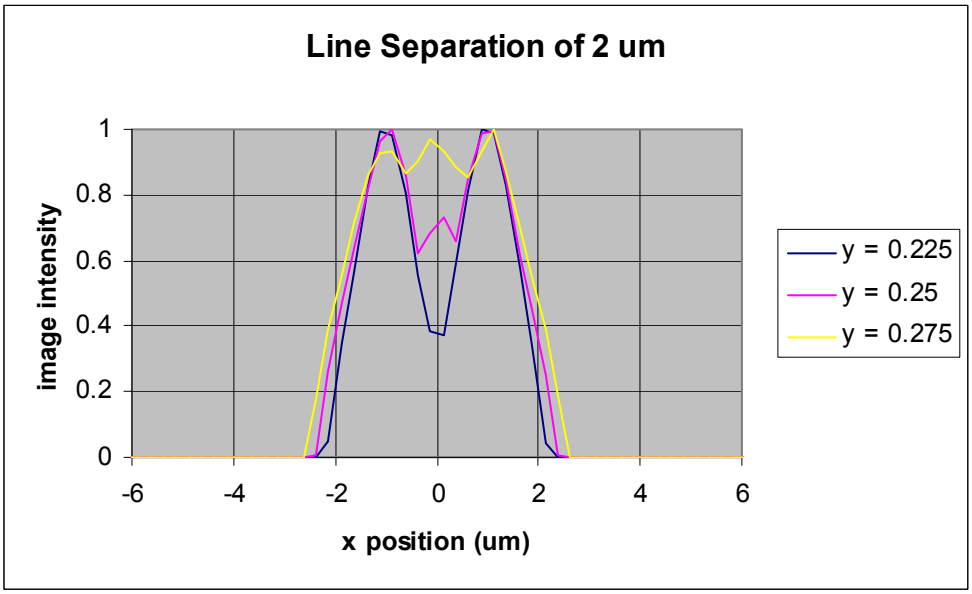

Figure E.4: Lines separated by 2 micrometer can be detected at an off-axis position of 0.260 millimeters (y=0.260 mm, FOV = 0.52 mm)

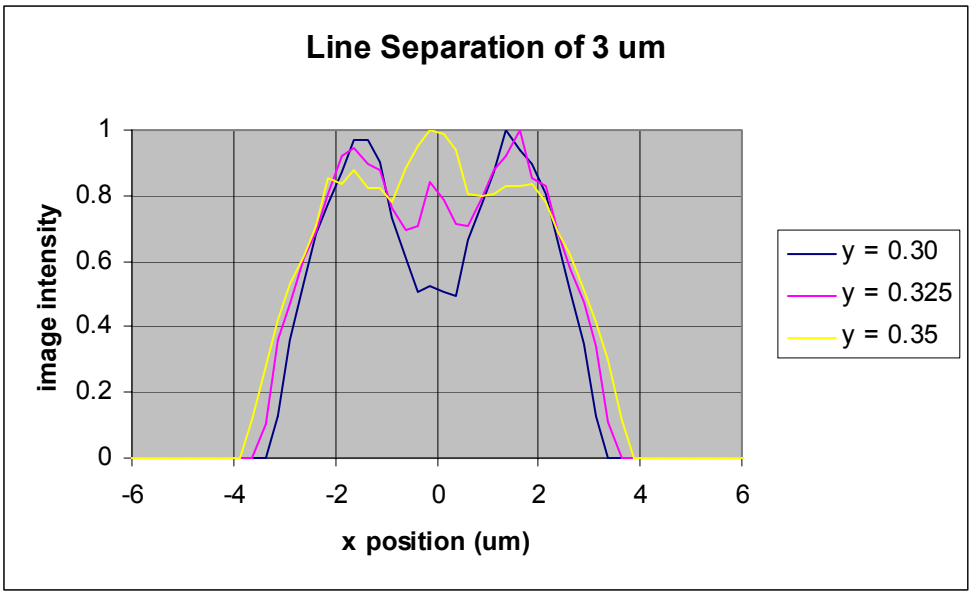

Figure E.5: Lines separated by 3 micrometer can be detected at an off-axis position of 0325 millimeters (y=0.325 mm, FOV = 0.65 mm)

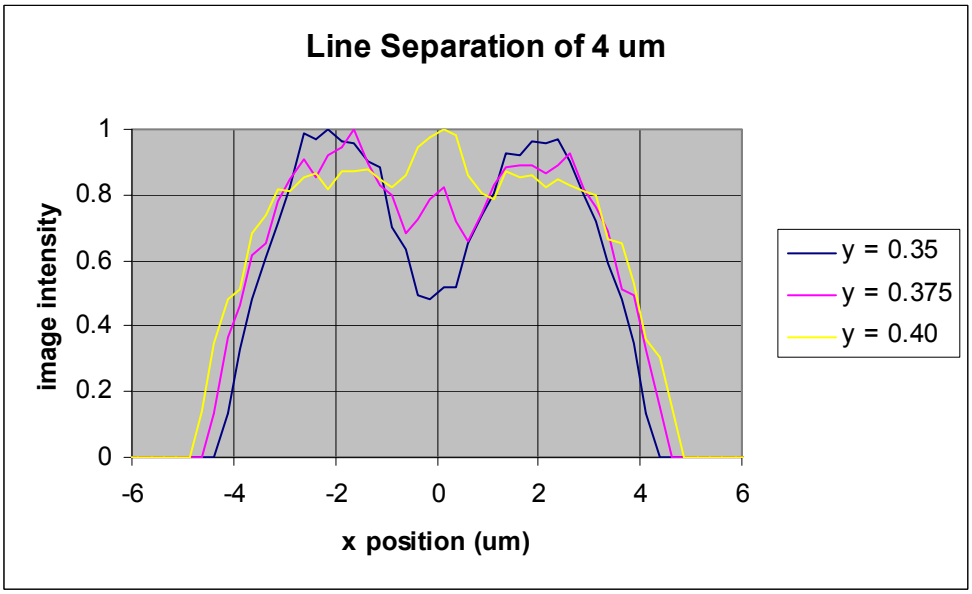

Figure E.6: Lines separated by 4 micrometer can be detected at an off-axis position of 0.375 millimeters (y=0.375 mm, FOV = 0.75 mm)

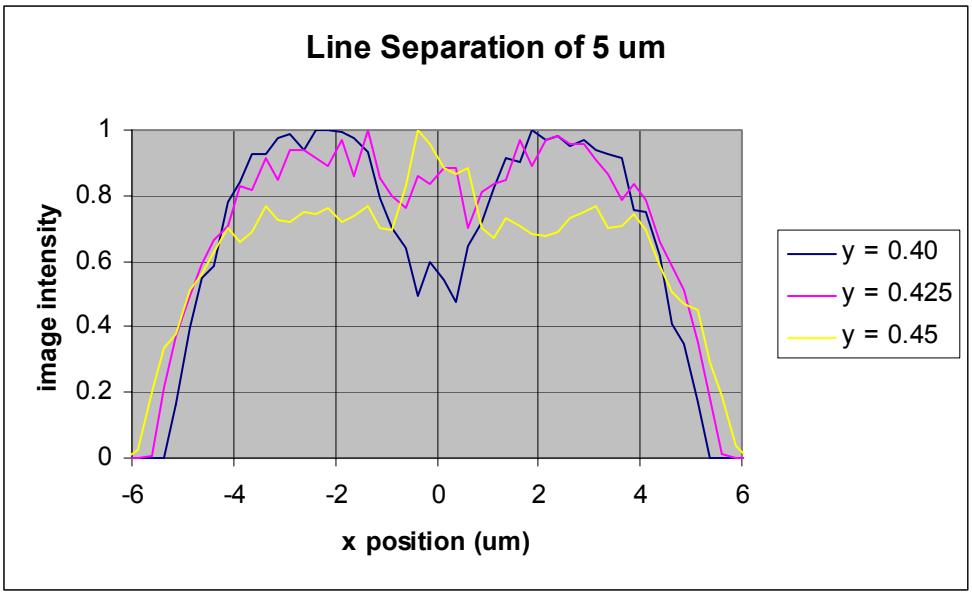

Figure E.7: Lines separated by 5 micrometer can be detected at an off-axis position of 0.415 millimeters (y=0.415 mm, FOV = 0.83 mm)

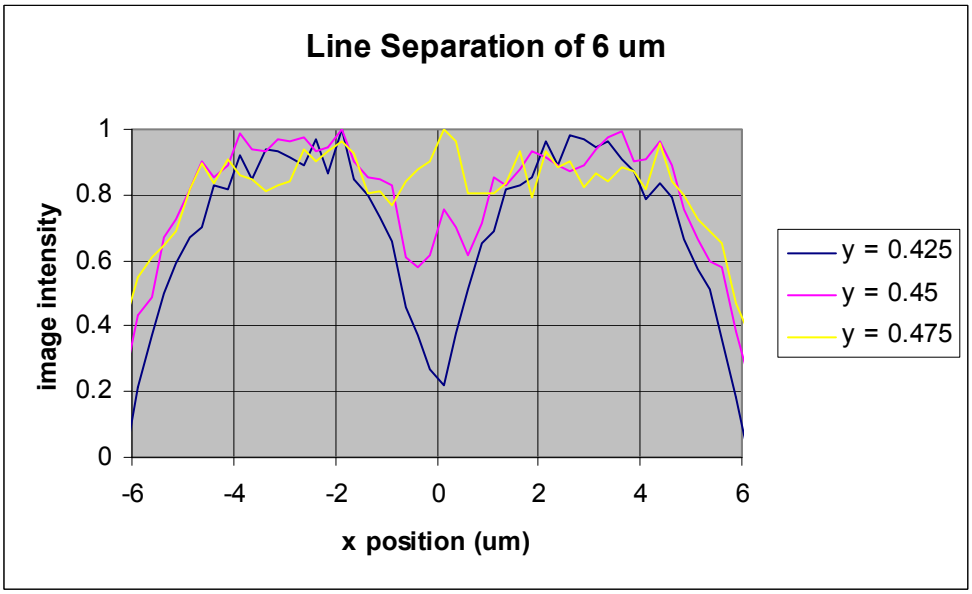

Figure E.8: Lines separated by 6 micrometer can be detected at an off-axis position of 0.45 millimeters (y=0.45 mm, FOV = 0.9 mm)

Edge detection method of looking at system resolution:

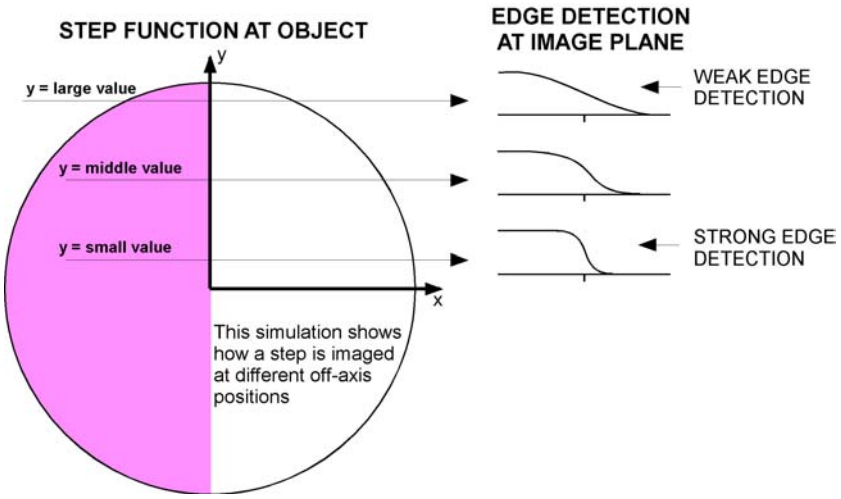

Figure E.9: Edge detection method

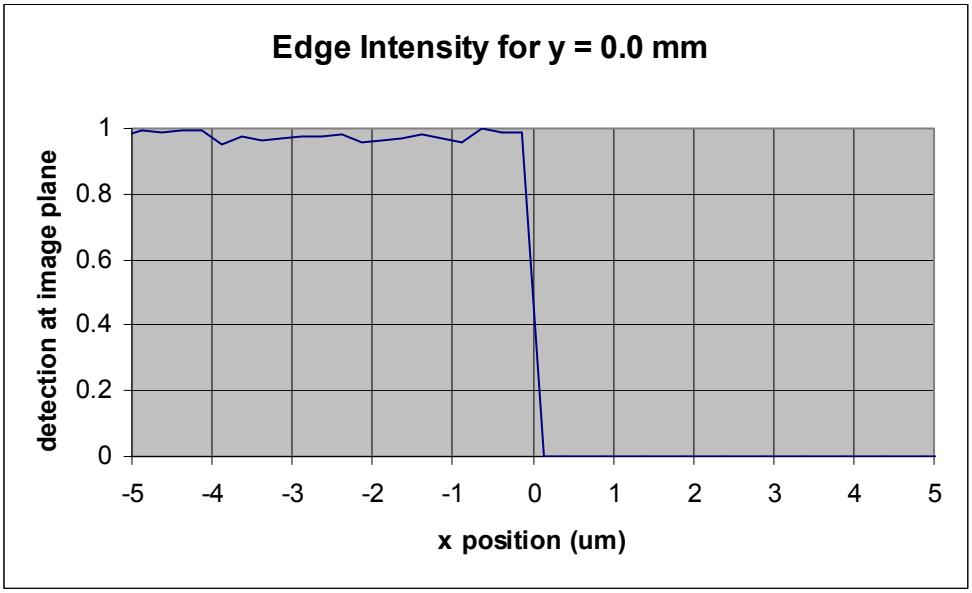

Figure E.10: Edge intensity for on-axis edge

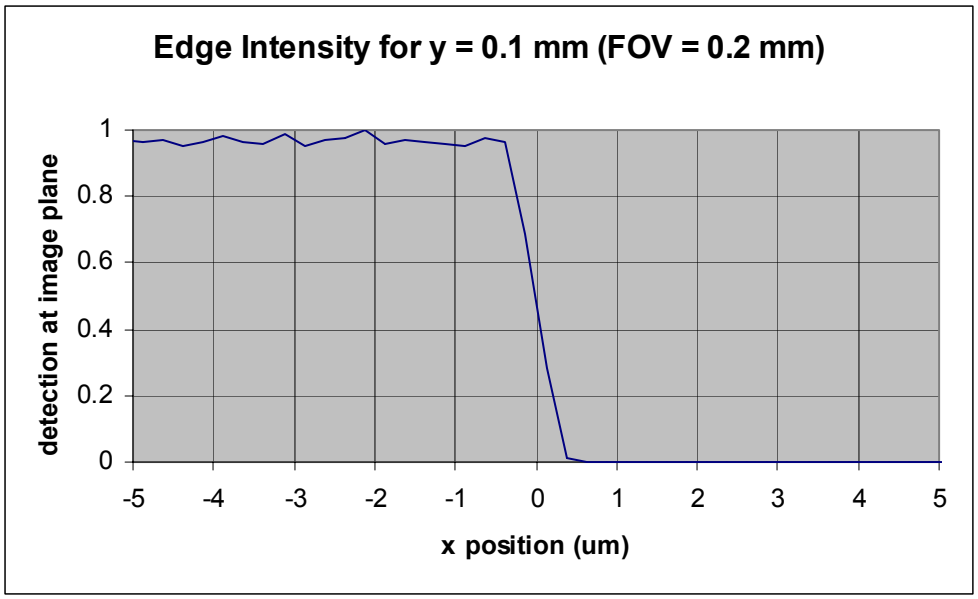

Figure E.11: Edge intensity for off-axis edge (y = 0.1 mm, FOV = 0.2 mm)

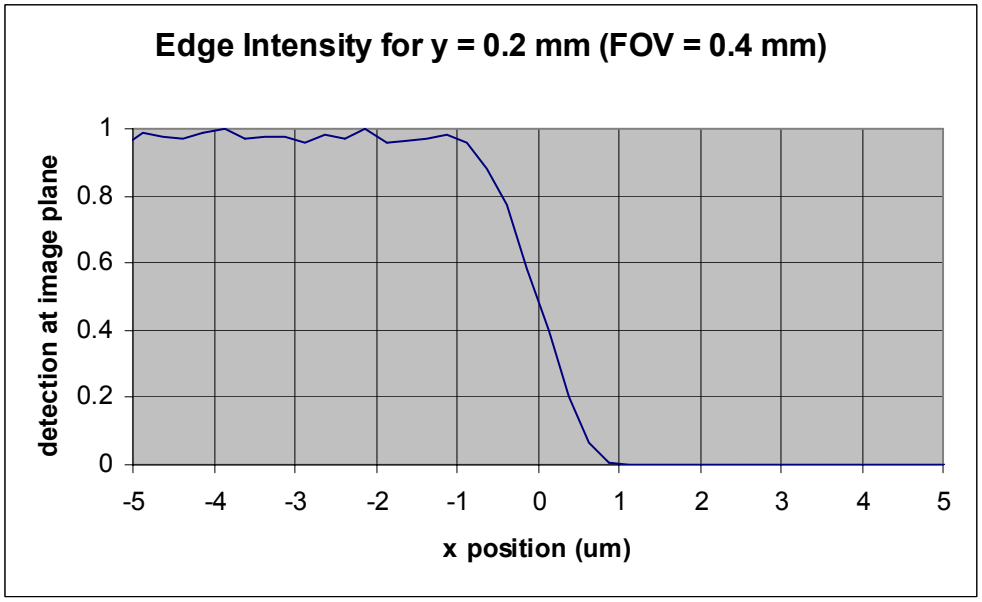

Figure E.12: Edge intensity for off-axis edge (y = 0.2 mm, FOV = 0.4 mm)

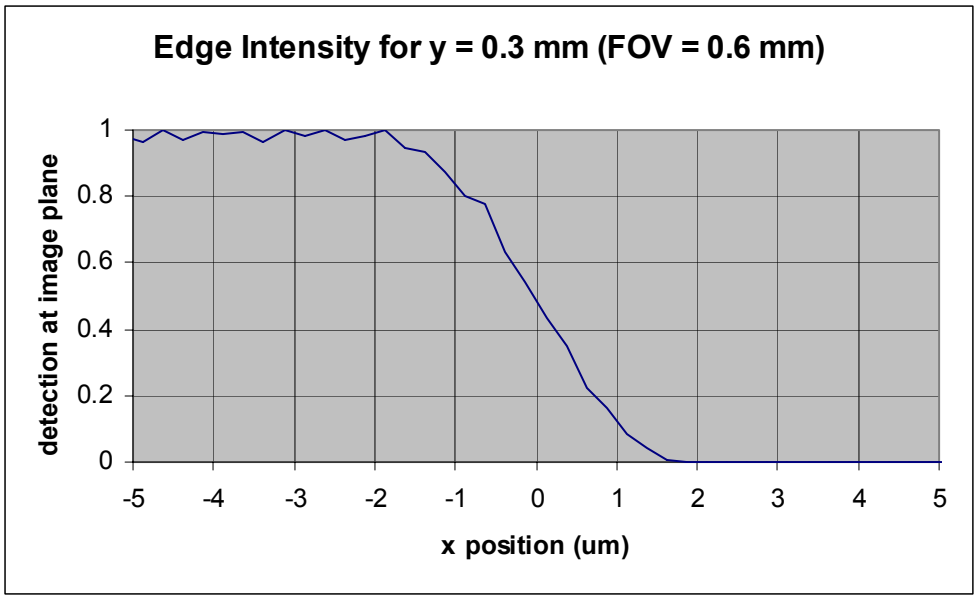

Figure E.13: Edge intensity for off-axis edge (y = 0.3 mm, FOV = 0.6 mm)

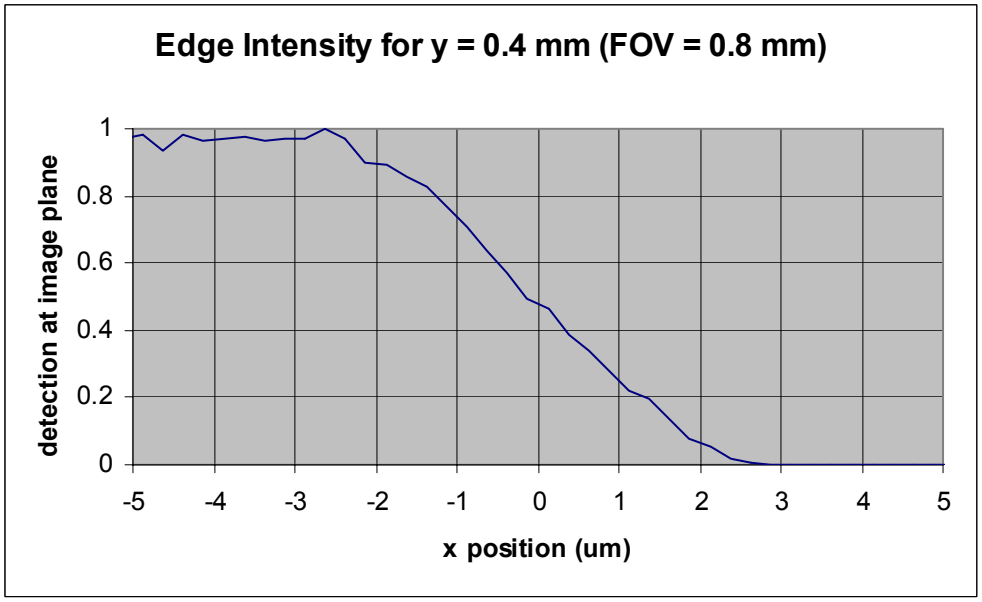

Figure E.14: Edge intensity for off-axis edge (y = 0.4 mm, FOV = 0.8 mm)

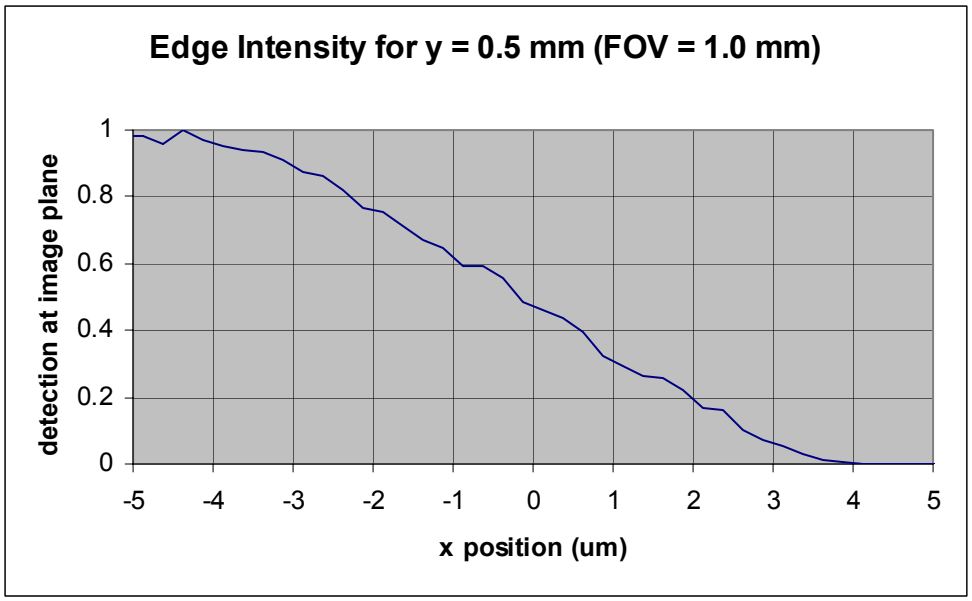

Figure E.15: Edge intensity for off-axis edge (y = 0.5 mm, FOV = 1.0 mm)

APPENDIX F: RAY TRACING TO DETERMINE SYSTEM BLUR

The blur at the image plane over the field of view (one millimeter diameter) was determined using ray tracing. Rays were emitted from points at the object plane. The rays were reflected off of both mirrors (optic C – the hyperbola & optic D – the ellipse). They were then captured at the image plane. Sixty rays (distributed equally over optic C) were emitted from each point on the object plane. We calculated the blur as the diameter that encompassed the entire imaged point (see Figure 2.6). Figure F-1 illustrates the ray tracing approach used for determining the system blur.

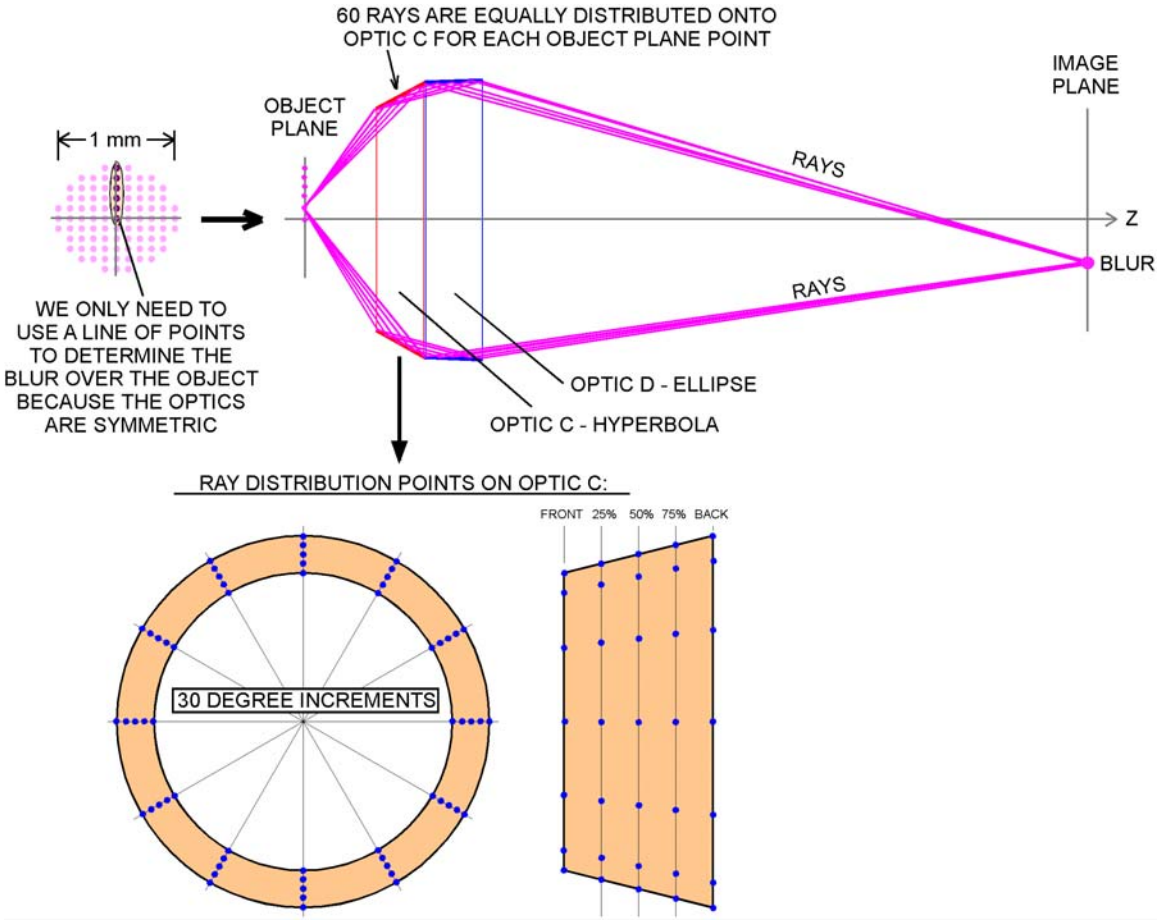

Figure F-1: Illustration of the ray tracing approach used for calculating system blur

The rays in the ray-tracing algorithm were represented using a point and a unit vector. The point represented the beginning of the ray, and the unit vector represented the direction of the ray. Due to the symmetric shape of the optical system, we only needed to image a line of points on the object plane. The blur over the field of view was obtained by revolving the blur results for the line of points about the z-axis. The algorithm flowchart for tracing the rays through the optical design is shown in Figure F-2. Several of the more difficult steps are discussed in the following paragraphs.

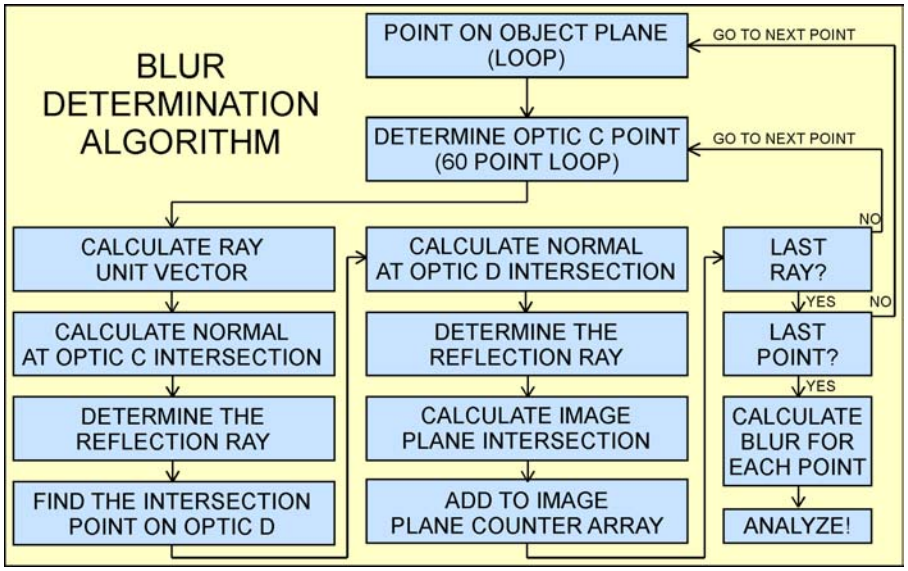

Figure F-2: ray-tracing flowchart

Calculating the normal at the ray/hyperbola intersection and the ray/ellipse intersection requires the slope of the optic at the point of intersection to be known. Figure F-3 shows the mathematics involved in finding this normal.

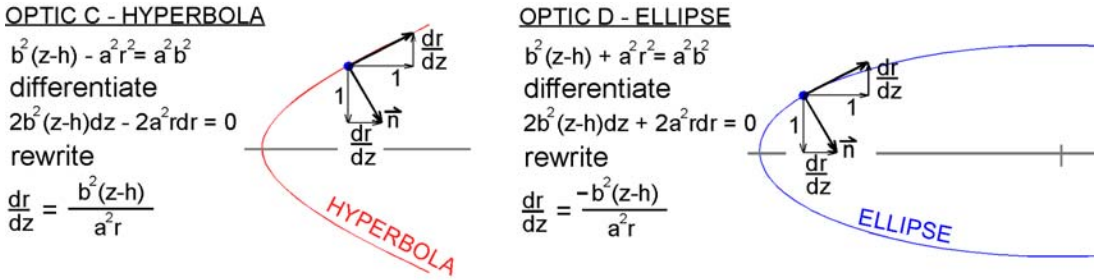

Figure F-3: Calculating the normal at an intersection

After a ray hits a mirror, it gets reflected off of the mirror. Hence, we need to determine the direction of the reflected ray. With the normal (a unit vector) and in-coming ray known, we can determine the reflected ray using simple vector algebra. The required vector algebra is shown in Figure F-4.

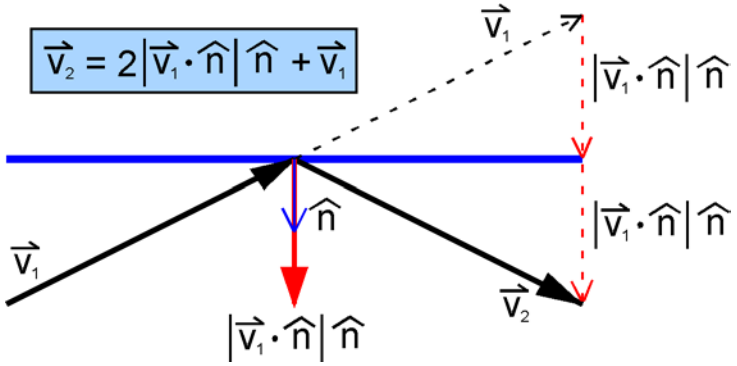

Figure F-4: Determining the reflected ray using vector algebra

The reflected ray from optic C should now intersect optic D. Calculating the intersection point requires solving a quadratic equation. Figure F-5 shows the mathematics necessary for calculating the intersection between a ray and optic D (hyperbola). If doing random ray tracing, then it would be necessary to find the intersection between a ray and optic C. For completeness, Figure F-6 shows the mathematic for calculating that intersection.

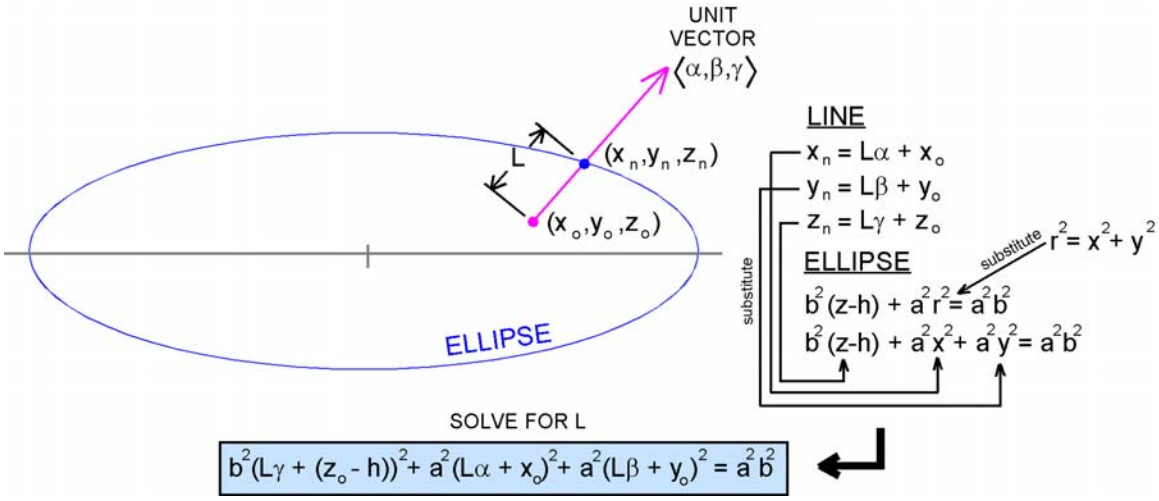

Figure F-5: Finding the intersection of a ray and optic D

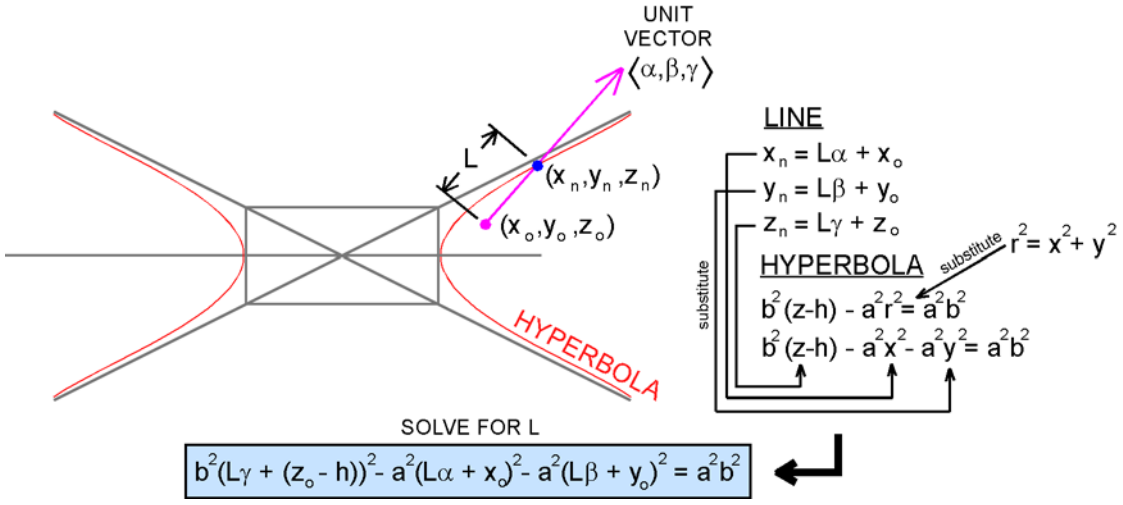

Figure F-6: Finding the intersection of a ray and optic C

After completing two reflections, a ray should intersect the image plane. Figure F-7 illustrates the mathematics needed for finding the intersection of a ray with the image plane. Capturing the ray at the image plane concludes the tracing of that ray.

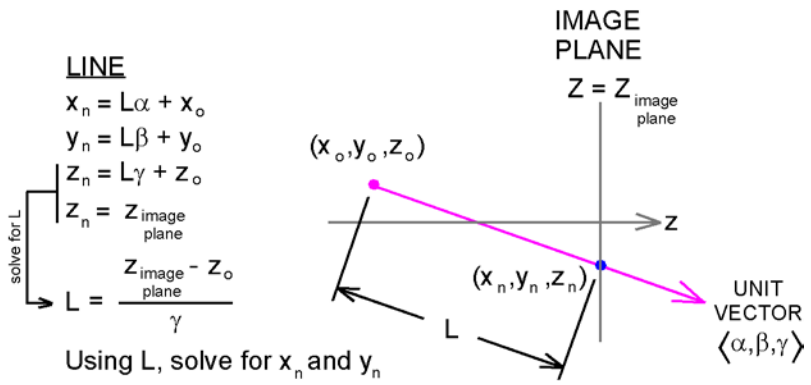

Figure F-7: Finding the intersection of a ray with the image plane

APPENDIX G: OPTICAL DESIGN – GEOMETRIC PARAMETERS – REVISED

The optical design parameters given in Appendix C represented an optical system that could not be easily made with our current fabrication equipment. The combined length of optic C and optic D exceeded the working volume of our best diamond turning machine. Therefore, the optical design was slightly shortened to alleviate this problem. The new optical design parameters are shown below. The ellipse and hyperbola parameters remain unchanged. NOTE: only values shown in red have been changed from the values shown in Appendix C.

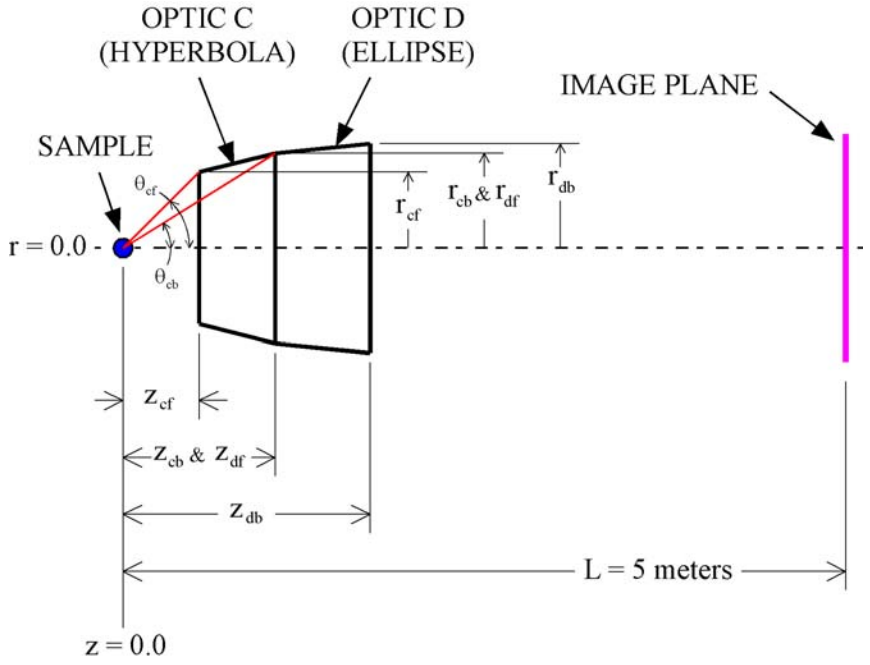

Figure C.1: Geometric parameters

Sample Location:

z_{sample} = 0.0 mm $\quad$ r_{sample} = 0.0 mm

Optic C:

Z_{cf} = 346.790052 mm $\quad$ r_{cf} = 33.832944 mm $\quad$ θ_{cf} = 5.5721599 degrees

Z_{cb} = 383.037896 mm $\quad$ r_{cb} = 36.349392 mm $\quad$ θ_{cb} = 5.4210000 degrees

Optic D:

Z_{df} = 383.037896 mm $\quad$ r_{df} = 36.349392 mm

Z_{db} = 422.913845 mm $\quad$ r_{db} = 37.041862 mm

Image Plane:

Z_{image} = 5000.0 mm

APPENDIX H: IMPROVING PERFORMANCE USING SURFACE DEVIATIONS

The hyperbolic and elliptical surfaces are ideal for imaging on axis points, but the resolution degrades rapidly as we move away from the optical axis. Deviating from the original conical surfaces (see Figure H-1) can increase on-axis blur, but lower off-axis blur. We used two different deviations methods to see if we could get sub-micrometer resolution over a one-millimeter field-of-view (i.e., flatten the resolution curve). We used polynomial surface representations[2] and Bezier surface representations[3]. We varied the surface parameters and searched the parameter space for improved resolution. Unfortunately, both approaches hurt near-axis performance too much (see Figure H-2). Based on our results, we decided to stay with the original conical surface design.

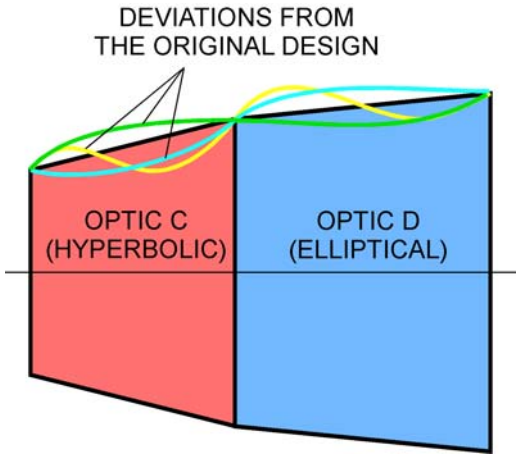

Figure H-1: Using surface deviations to improve the optical performance of the system

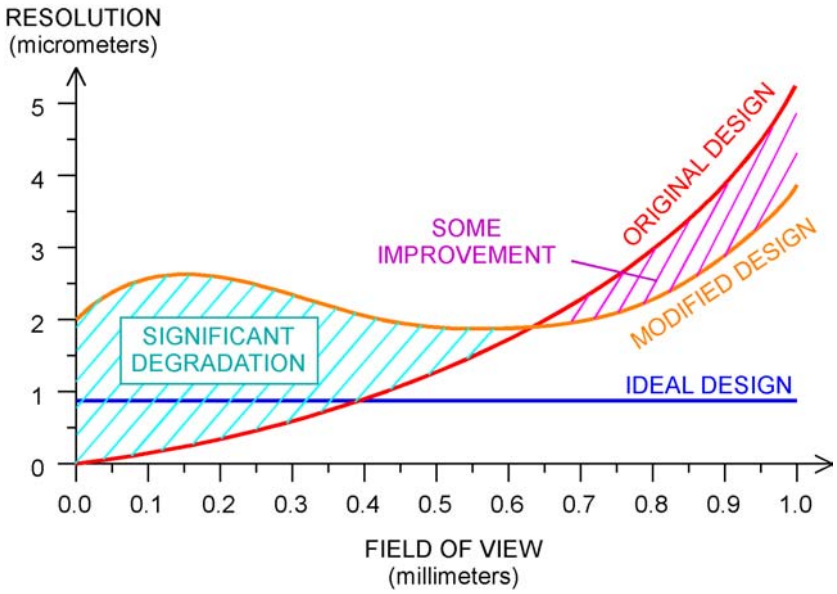

Figure H-2: Changes in resolution caused by surface deviations

[2] Analysis performed by Michael Pivovaroff
[3] Analysis performed by Walter Nederbragt